A geology-based 3D velocity model of the Amatrice Basin (Central Italy)

Published Version:
Livani M., Scrocca D., Gaudiosi I., Mancini M., Cavinato G.P., de Franco R., et al. (2022). A geology-based 3D velocity model of the Amatrice Basin (Central Italy). ENGINEERING GEOLOGY, 306, 1-16 [10.1016/j.enggeo.2022.106741].

Availability:
This version is available at: https://hdl.handle.net/11585/899022 since: 2024-05-24

Published:
DOI: http://doi.org/10.1016/j.enggeo.2022.106741

Highlights

- A new detailed 3D geological model, with related geophysical parameters, of the uppermost hundreds of meters of the Amatrice area has been elaborated;
- the model has been calibrated by processing the ellipticity curves of the Rayleigh fundamental mode at four chosen sites;
- the model predicts correctly the amplitude and frequency of arriving waves;
- the model could help in predicting possible focusing and/or amplification effects due to the morpho-litho-stratigraphic setting of the near surface geological structures;
- the proposed modeling approach allows to define more realistic seismic hazard scenarios being also exploitable in other similar seismic areas.

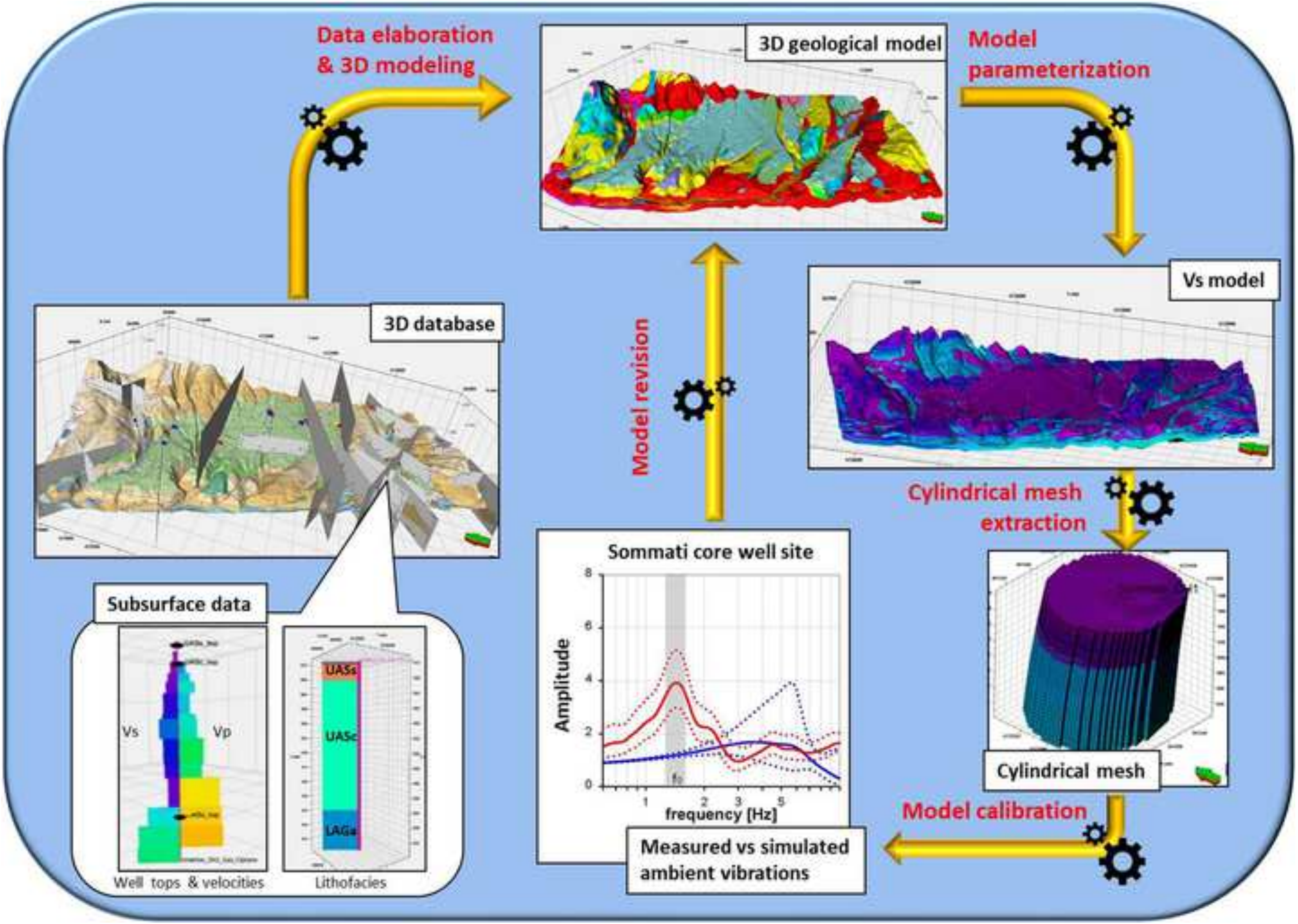
Data elaboration
& 3D modeling
3D geological model
Model
parameterization
Vs model
3D database
Model revision
Cylindrical mesh
extraction
Subsurface data
Vs
Vp
Well tops & velocities
UASs
UASc
LAGa
Lithofacies
Sommati core well site
Amplitude
8
6
4
2
0
1
2
3
5
f0
frequency [Hz]
Measured vs simulated
ambient vibrations
Cylindrical mesh
Model calibration

3D geological modeling, a new approach in seismic hazard assessment studies: insights from the Amatrice case study (central Italy).

Michele Livani[a], Davide Scrocca[a,*], Iolanda Gaudiosi[b], Marco Mancini[b], Gian Paolo Cavinato[a], Roberto de Franco[c], Grazia Caielli[c], Gianluca Vignaroli[b,d], Alessandro Romi[e], Massimiliano Moscatelli[b].

[a] Istituto di Geologia Ambientale e Geoingegneria, Consiglio Nazionale delle Ricerche, c/o Dipartimento di Scienze della Terra, Università Sapienza, P. le A. Moro 5 - 00185, Roma, Italy

[b] Istituto di Geologia Ambientale e Geoingegneria, Consiglio Nazionale delle Ricerche, Area della Ricerca di Roma 1, Strada Provinciale 35d 9 - 00010, Montelibretti (RM), Italy

[c] Istituto di Geologia Ambientale e Geoingegneria, Consiglio Nazionale delle Ricerche, Piazza della Scienza,1 - 20126 Milano, Italy

[d] Dipartimento di Scienze Biologiche, Geologiche e Ambientali, Università degli Studi di Bologna, Via Zamboni 67 - 40127, Bologna, Italy

[e] Schlumberger Italiana, Via dell'Unione Europea, 4 - Torre Beta 20097 San Donato Milanese (MI), Italy

***Corresponding author:** Davide Scrocca

E-mail: davide.scrocca@igag.cnr.it

Abstract

The Amatrice area (central Italy) falls in a high seismic hazard region, which has been struck by several disastrous earthquakes. The recent 2016-2017 seismic sequence, with several earthquakes of magnitude Mw greater than 5, caused extensive damage and 299 victims, reaffirming the importance of activities devoted to the seismic risk prevention in an effective territorial planning.

In this paper we present a detailed 3D geological model, with related geophysical parameters, of the uppermost hundreds of meters (maximum depth about 200 meters) of the Amatrice Basin subsoil. Geological maps, cross-sections, and morphological data (Digital Elevation Model) have been integrated with subsurface geological and geophysical data (e.g., core-well data and seismic noise measures) and models obtained by the interpretation of surface and well geophysical measurements, like S-wave (Vs) and P-wave (Vp) velocities. All data have been georeferenced and uploaded into a 3D geological modeling software, where faults, stratigraphic boundaries and geophysical attributes have been digitized, checked, hierarchized, and modeled. A posteriori calibration of the 3D reconstructed model has been operated by comparing the modeled seismic responses of some extracted volumes with those obtained by environmental noise measurements (i.e., Horizontal-to-Vertical Spectral Ratio analysis, HVSR). The final 3D model correctly reproduces the amplitude and frequency of arriving waves in the Amatrice area, thus allowing an evaluation of possible focusing and/or amplification effects due to the morpho-litho-stratigraphic setting of the near surface geological features (i.e., Quaternary cover deposit and pre-Quaternary rocky substratum). The proposed 3D modeling approach represents a promising general methodology for developing more realistic seismic hazard scenario, useful for allowing an effective territorial planning.

Keywords: 3D geological model, seismic hazard assessment, seismic risk prevention, Amatrice Basin, Laga Basin, central Apennines.

1 Introduction

In last decades, the advent of the three-dimensional (3D) geological modeling software gave to geologists a new tool to effectively represent the subsurface. A detailed 3D geological and mechanical model is an important tool for assessing the seismic hazard of an area. As an example, compared to classic two-dimensional (2D) models, 3D seismogenic source models can provide a more realistic prediction of the expected ground shaking as well as of its spatial distribution (e.g., Boncio et al., 2004). Defining 3D geometries of rock bodies and the spatial distribution of their mechanical properties allow running physically based numerical simulations (e.g., Mazzieri et al., 2013; Smerzini and Pitilakis, 2018) and, consequently, investigating their role in influencing the upward propagation of seismic waves, highlighting the possible occurrence of focusing, reflection, refraction and/or amplification effects. In addition, a 3D geological model can be used for predicting amplitude and frequency of the arriving seismic waves (e.g., Magistrale et al., 1996; Süss et al., 2001),

In this framework, our study area (the Amatrice Basin, central Italy), provides a remarkably interesting case study for reconstructing a 3D geological model due to the large amount of available seismological, geological and geophysical data. The Amatrice Basin (Cacciuni et al., 1995; Vignaroli et al., 2019) is a NW-SE-trending intermountain depression in the axial part of the central Apennines (Fig. 1). For this area, at the state of art, a 3D fully parameterized model in terms of mechanical parameters is still missing.

The study area has been historically affected by moderate-to-large earthquakes that produced extensive damage and many victims (e.g., the 1639 and 2016-2017 seismic sequences; Tiberi Romano, 1639; Galli et al., 2016; Chiaraluce et al., 2017; Pizzi et al., 2017; Rovida et al., 2019; and references therein) (Fig. 1). Recently, it has been struck by a seismic sequence started on the 24th August 2016 (with the Amatrice earthquake of magnitude Mw 6.0) due to the activation of a complex system of extensional faults. Numerous earthquakes of magnitude Mw> 5 have been recorded in the period between 24th August 2016 and 18th January 2017 (e.g., Chiaraluce et al., 2017; Improta et al., 2019; Michele et al., 2020 and references therein).

After the 2016-2017 events, the Amatrice area has been the subject of numerous research projects, including surface geological surveying and data collection (e.g., V_s and V_p data) activities (e.g., Vignaroli et al., 2019; 2020; Mancini et al., 2020) aimed at the seismic microzonation (EmerTer Project Working Group, 2018; Chiaretti & Nibbi, 2018). Seismic microzonation provided seismic hazard estimates at the municipality scale, based on shallow geological/geotechnical conditions and site-dependent constraints, for the design of new settlements and for interventions of retrofit and reconstruction (Hailemikael et al., 2020). Furthermore, a 2D and 3D numerical modeling of the site effects for the main hamlet of the entire Amatrice municipality has been also attempted (Gaudiosi et al, 2021; Moscatelli et al., 2020; Razzano et al., 2020), while a new 3D geological modeling project, named RETRACE-3D, has been launched. The latter aimed at obtaining, by interpreting seismic lines and well data, a 3D seismotectonic and stratigraphic characterization of the Amatrice Basin (Di Bucci et al., 2021; RETRACE-3D Working Group, 2021).

The aim of our study is to contribute to a more effective seismic hazard assessment of the Amatrice area by providing an accurate (resolution from 5m up to 1m in-depth and 5m in plan) 3D geological and mechanical model of a shallow portion (maximum depth about 200 meters) of subsoil, joining the previously available existing models. Our model integrates surface and subsurface (some hundred meters deep) geological data, as well as geophysical parameters, setting the ground for a proper evaluation of the local seismic response in tectonically active geologically complex areas. The methodology here proposed could bridge the gap between deep seismotectonic reconstructions typical of seismic zonation and characterizations of shallow portions of subsoil in seismic microzonation studies.

2 Geological setting

The study area is part of the central Apennines, an eastward-migrating fold-and-thrust belt, developed since the upper Oligocene above the westward subducting Adria plate (Malinverno & Ryan, 1986; Ricci Lucchi, 1986; Patacca et al., 1990; Boccaletti et al., 1990; Doglioni, 1991; Argnani & Ricci Lucchi, 2001; Cosentino et al., 2010). Along the belt axial zone, the foredeep Laga Basin is located, which is bounded by the Gran Sasso thrust to the south, the Sibillini thrust to the west, and the Montagna dei Fiori-Montagnone anticline to the east (Fig. 1).

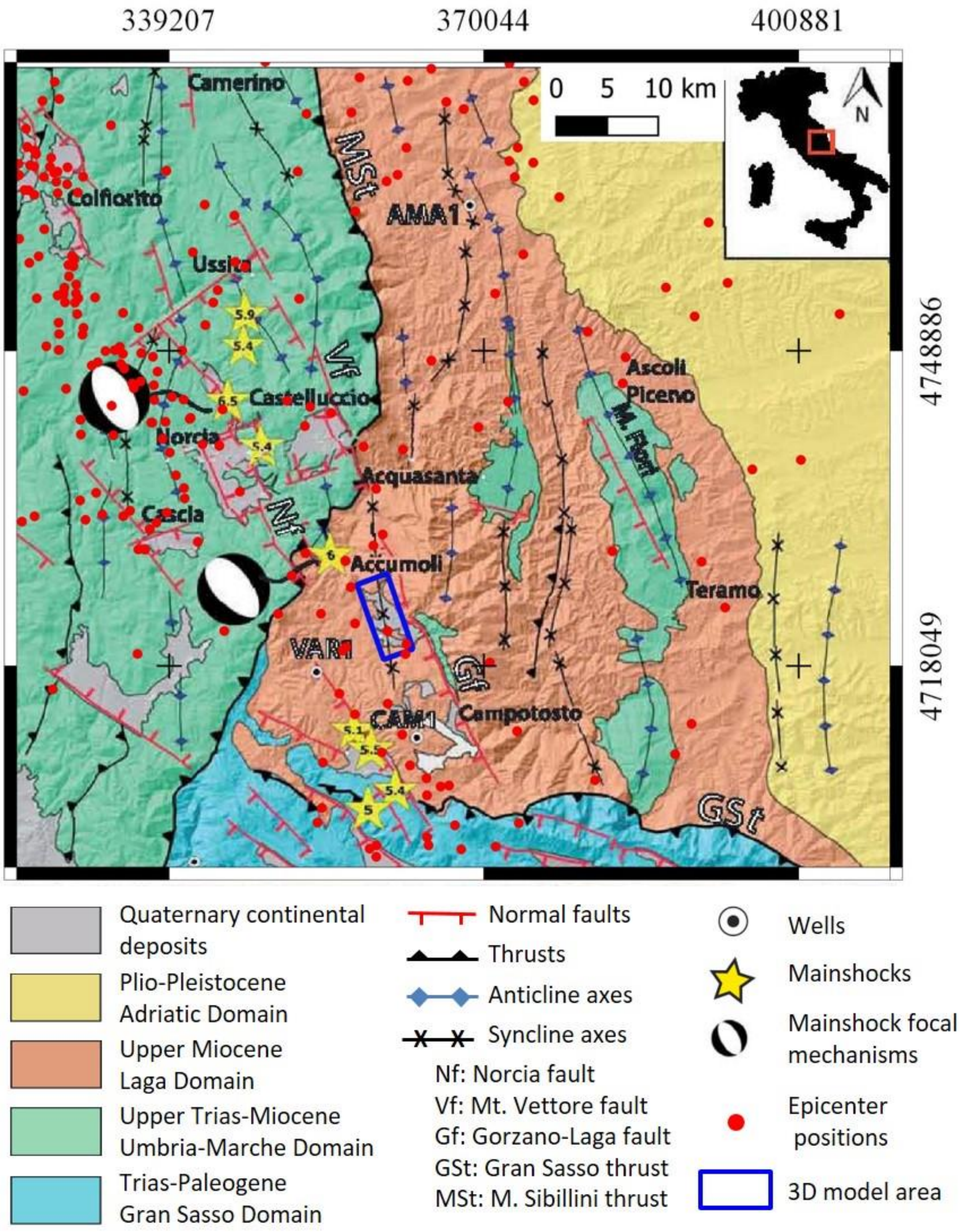

Figure 1: Geological and seismicity map of the study area (modified after Porreca et al., 2018). Yellow stars represent the epicenter positions of the 2016 seismic event with Mw>5. The focal mechanisms mainshocks (Mw 6.0 and 6.5) and the positions of the Amatrice 1 (AMA1), Campotosto 1 (CAM1) and Varoni 1 (VAR1) wells are shown. The position of the Gran Sasso and Sibillini regional thrusts (GSt and MSt, respectively), and of the Vettore (Vf), Norcia (Nf), and Gorzano-Laga (Gf) extensional fault systems are also shown. The blue rectangle indicates the Amatrice area, which is detailed in figure 4.

Facies and physical stratigraphy, analysis of thermal history, seismic line interpretations and balanced cross sections allowed a detailed reconstruction of the stratigraphy and the time-space evolution of the Laga Basin, thus representing a key area to understand the most recent evolution of the central Apennines (Koopman, 1983; Centamore et al., 1991; 1992; Artoni, 2003, 2007; Moscatelli, 2003; Moscatelli et al., 2004; Scisciani & Montefalcone, 2005; Casero & Bigi, 2006; Bigi et al., 2006, 2009; Stanzione et al., 2006; Aldega et al., 2007; Milli et al., 2007, 2009; Cosentino et al., 2010).

The Laga Basin is filled by more than 2000-m thick deep-sea turbidite succession, named Laga Formation (Mutti & Ricci Lucchi, 1972; Mutti et al., 1978; Mutti & Sonnino, 1981; Milli et al., 2007, 2009; Marini et al., 2015, 2016). It consists of an alternation of lithofacies that vary from arenaceous and pelitic-arenaceous to marly (e.g., Milli et al., 2007; 2009; Mancini et al., 2020) grouped into three main members: pre-evaporitic (upper Tortonian-lower Messinian), evaporitic (middle Messinian), and post-evaporitic (upper Messinian) ones (Roveri at al., 2001).

A 1200-m thick pre-evaporitic Laga Formation has been identified by the stratigraphy of the Campotosto 1 and Varoni 1 wells (locations in figure 1) and the interpretation of some seismic reflection profiles (e.g., Bigi et al., 2011; Porreca et al., 2018). The Laga Formation lies above the *“Marne con Cerrogna”* and *“Marne ad Orbulina”* Formations, a Langhian to lower Messinian pelagic succession that is today exposed at the footwall of the Gorzano-Laga Fault (in the eastern edge of the study area) (Fig. 1). The Laga Formation is topped by a succession of lower Pleistocene to Holocene continental deposits consisting of sandstones and conglomerates of alluvial fans and fluvial terraces, forming the Amatrice Basin (e.g., Centamore et al., 1991, 1992; Cacciuni et al., 1995; Vignaroli et al., 2019; 2020; Mancini et al., 2020) (Fig. 2).

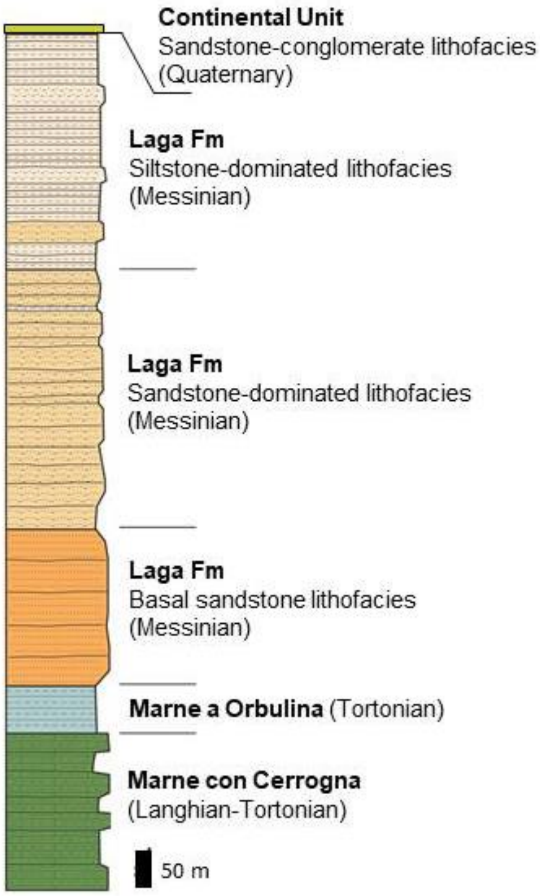

Figure 2: Synthetic stratigraphic column of the middle Miocene-to-recent sedimentary interval (modified after Mancini et al., 2020).

The Laga Basin originated since the Messinian time (Ricci Lucchi, 1986; Roveri et al., 2002, 2003; Manzi et al., 2005; Bigi et al., 2006; Milli et al., 2007, 2009; Bigi et al., 2009; Cosentino et al., 2010) and evolved with the activation of major out-of-sequence thrust systems in the late Messinian-early Pliocene time (e.g., Billi & Tiberti, 2009) when, due to the compressional tectonic activity, the Laga Formation filled the confined foreland basin. Since the Pliocene time, the post-orogenic phase leads to the activation of the main extensional faults (e.g., Malinverno & Ryan, 1986; Cavinato & De Celles, 1999) and the formation of fault-bounded intra-mountain basins that disarticulate the old orogenic framework (e.g., Cavinato, et al., 2002; Giaccio et al., 2012; Mancini et al., 2012; Pucci et al., 2015; Nocentini et al., 2017).

Today, this portion of central Apennines, where the study area is located, is a high-hazard region affected by post-orogenic extension occurring along Quaternary normal faults (e.g., Cavinato and De Celles, 1999; Galadini, 1999; Galadini & Galli, 2003, Mancini et al. 2019, Vignaroli et al., 2019; 2020; and reference therein) and causing widespread historical and instrumental seismicity (CSI, Castello et al., 2006; ISIDe working group, 2007; CPTI15 V2.0, Rovida et al., 2019; 2020) (Fig. 1).

The 2016-2017 seismic sequence in the Amatrice area consisted of many earthquakes aligned along an NNW-SSE-trending, 60 km-long normal fault system (e.g., Scognamiglio et al., 2016; Chiaraluce et al., 2017; Improta et al., 2019; Michele et al., 2020; and references therein). The seismic sequence was characterized by three mainshocks: Mw 6.0 (on 24th August) located near the Amatrice town; Mw 5.9 (on 26th October) at the northernmost border of the sequence, near the Visso town; Mw 6.5 (on 30th October) that occurred right in the middle of the fault system already activated in August, near the Norcia town (Fig. 1). In the same area, another catastrophic and remarkably similar seismic event occurred in 1639, with an estimated Mw 6.2 mainshock (Tiberi Romano, 1639; Rovida et al., 2019; 2020). Galli et al. (2016) suggest that the 1639 seismic event could have been generated by the same seismogenic fault that ruptured in 2016. In the past, the Amatrice and surrounding areas have been struck by other moderate-to-large seismic sequences, as the 1703 L'Aquila (estimated Mw 6.7 mainshock; Rovida et al., 2019; 2020), the 1997 Colfiorito (Mw 6.0 mainshock; Deschamps et al., 2000; Ripepe et al., 2000), and the 2009 L'Aquila (Mw 6.3 mainshock; Scognamiglio et al., 2010; Lucente et al., 2010; Chiaraluce et al., 2011; Herrmann et al., 2011; Valoroso et al., 2013; Lavecchia et al., 2017) sequences. Like the 2016-2017 sequence, the 1997 Colfiorito and the 2009 L'Aquila sequences were characterized by the occurrence of multiple events that activated 5-15 km long, southwest-dipping normal fault segments (Chiaraluce et al., 2017).

3 Data and methods

This work is based on a multidisciplinary approach that integrates geological and geophysical datasets (Fig. 3).

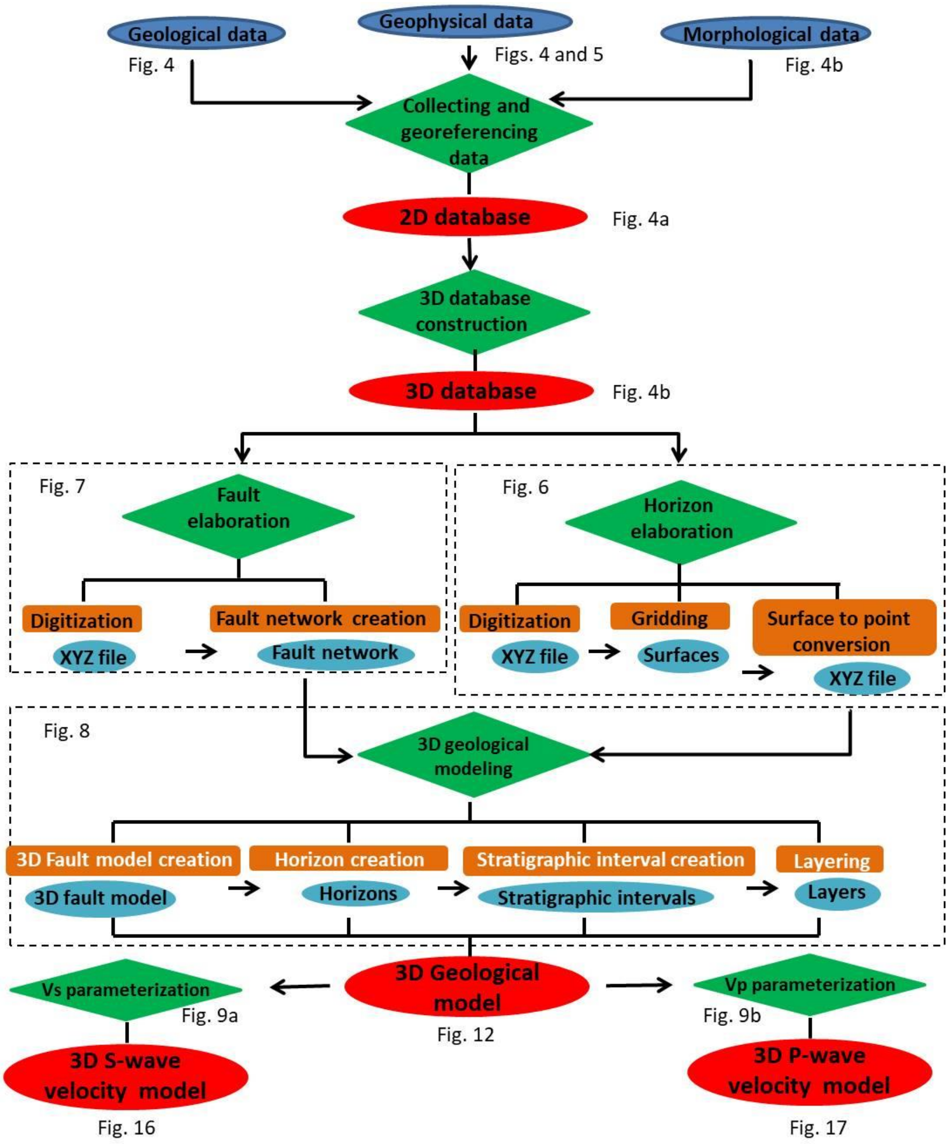

Figure 3: Workflow chart. Main processes (green diamonds) and their sub-processes (brown rectangles), primitive (blue ellipses) and derived (light blue ellipses) data, realized databases and models (red ellipses) are represented. The contextualization of some figures in this paper is indicated.

3.1 Data collection

Geological and geophysical data derive from fieldworks and surveys performed at 1:5.000 scale and from published works on the area struck by 2016-2017 seismic sequence (Chiaretti & Nibbi, 2018; EmerTer Project Working Group, 2018; Milana et al., 2019; Vignaroli et al., 2019; 2020; Mancini et al., 2020; Del Gaudio et al., 2021). This geological dataset provides information on (i) nature, thickness and distribution of the main lithotypes, and (ii) orientation, geometry and kinematics of the main tectonic structures (e.g., faults and their associated fracture network). Surface geological data have been integrated with data from 16 Down-Hole (DH) measurements, 8 associated Multichannel Analyses of Surface Waves (MASW), to some of which (i.e., Cascello, Collecreta, Prato MASW) V_p values deriving from some seismic refraction profiles acquired along the same traces have been associated, and 15 Horizontal-to-Vertical Spectral Ratio analyses (HVSR or 2D array). DHs reach a maximum depth of about 50 meters, while MASWs and 2D arrays in some cases exceed 200 meters in depth (Table 1), allowing to constrain the deeper parts of the geophysical model.

A 5 m-resolution digital elevation model (DEM), deriving from the 1:5.000-scale Regional Technical Map of the Rieti Province has been used as topographic base (Fig. 4).

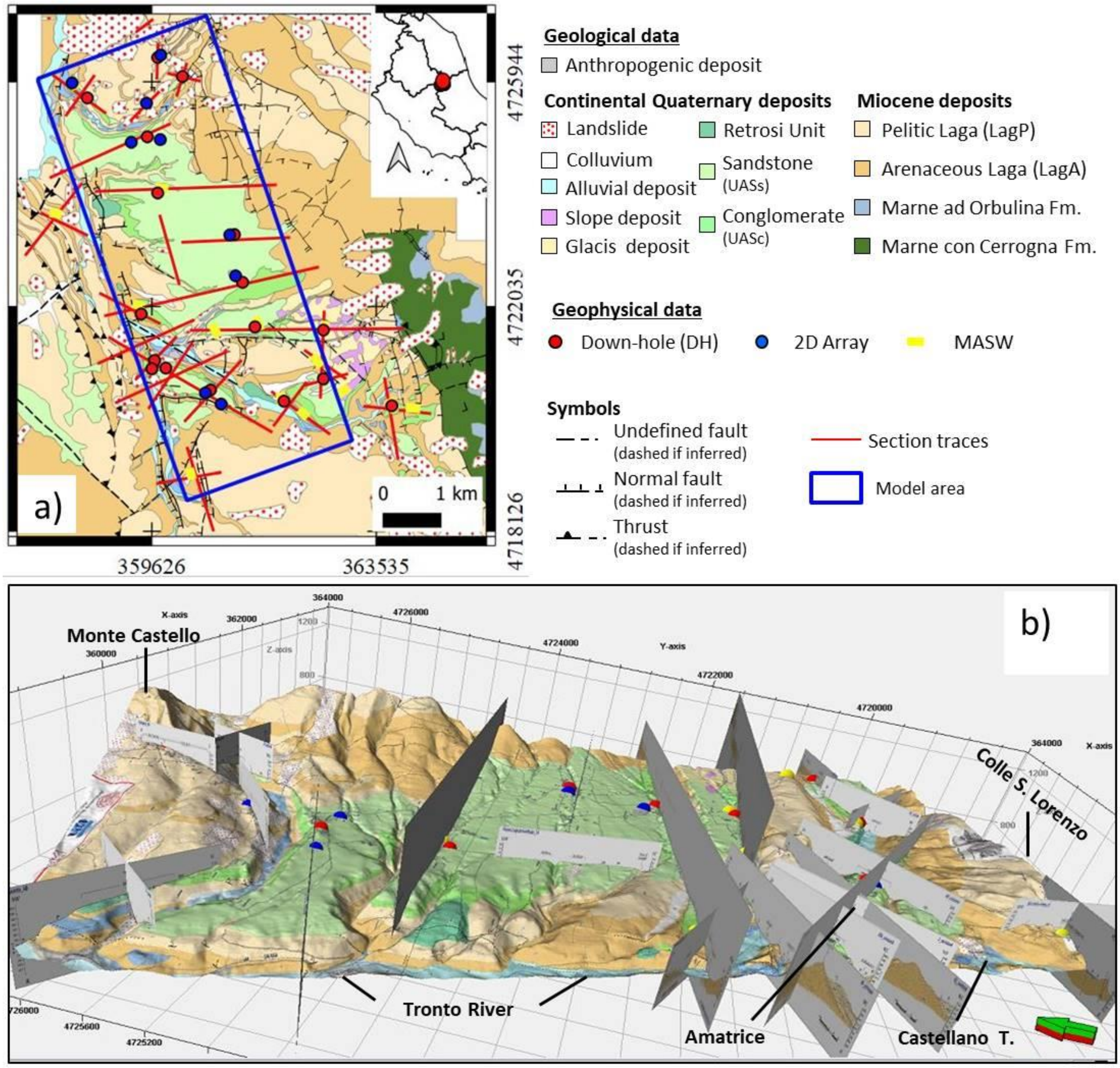

Figure 4: Used data. (a) 2D GIS image of geological (geological map and cross-sections by Vignaroli et al., 2019) and geophysical data (general geological framework in figure 1); (b) 3D view of geological and geophysical data in the model area (blue rectangle in figure 1). The geological map is projected on a 5-m resolution Digital Elevation Model. The overlapped points represent the DH (red points), 2D array (blue points), and MASW (yellow points) locations. See figure 3 to contextualize figures in the workflow.

DH data provided stratigraphic information, like lithofacies tops (classified according to Mancini et al., 2020, for the Quaternary deposits, and Vignaroli et al., 2019, for the Messinian Laga Formation) and velocity information (i.e., V_s and V_p velocities) of the drilled deposits (Figs. 5b, 5c, 5d). Finally, MASW (Fig. 5e) and 2D array (Fig. 5f) data have been used for constraining the wave velocities for each lithofacies (Table 1).

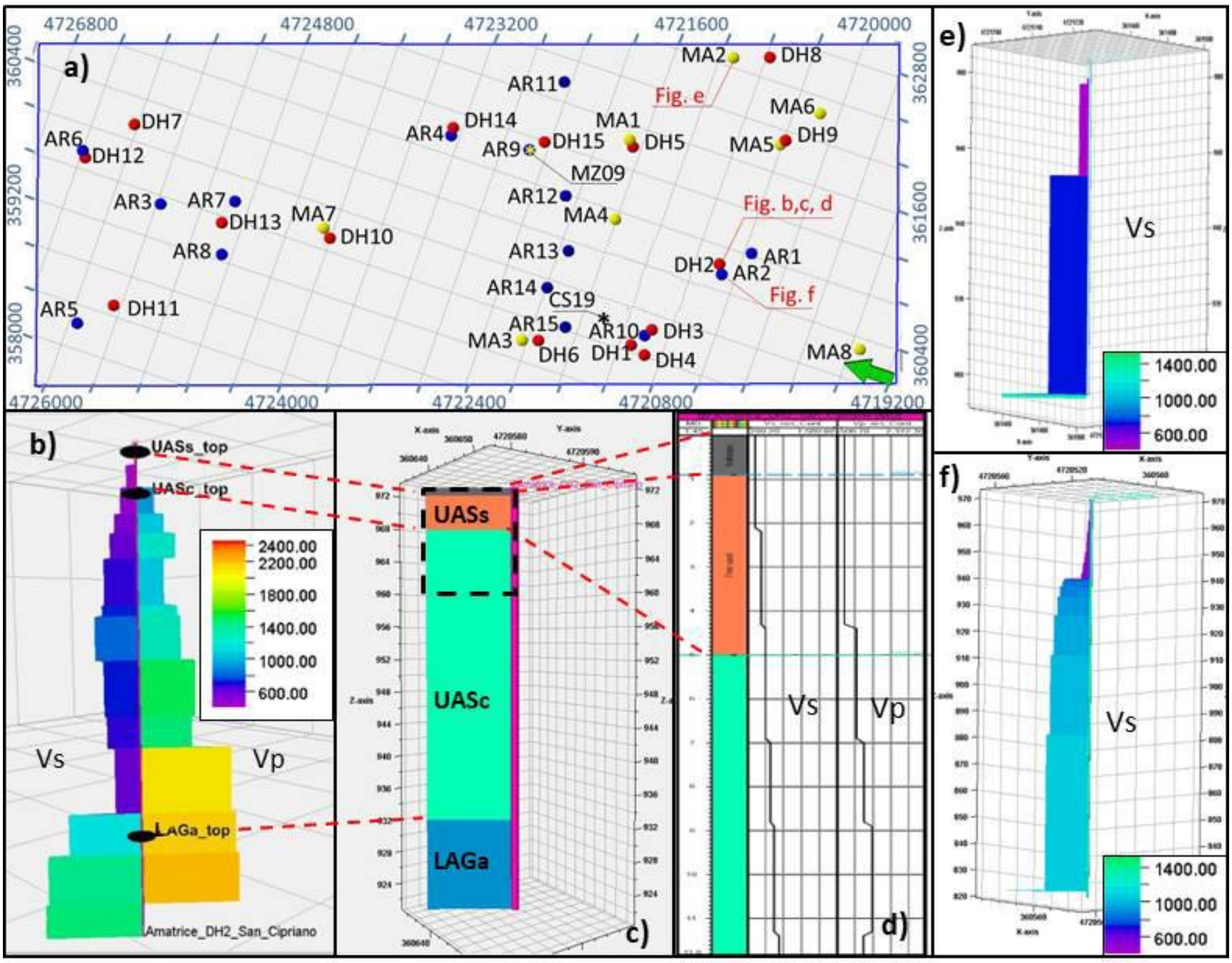

Figure 5: Subsoil geological and geophysical data. (a) Location map of seismic stations (black and yellow asterisks) and DH (red points), 2D array (blue points) and MASW (yellow points) measurement points; a code is associated with each measurement point (see corresponding extended names in table 1); the green arrow points north. (b) Lithofacies tops (black ellipses: UASs, Quaternary sandstones; UASc, Quaternary conglomerates; LAGa, arenaceous Laga) and velocity data (V_p and V_s) in the Amatrice-San Cipriano DH, also named Amatrice DH2; (c) litofacies in the Amatrice-San Cipriano DH (grey, anthropic; orange, fine sand; light blue, gravel and sand; blue, sandstone and siltstone); (d) well section window of a portion of the Amatrice-San Cipriano DH; (e) Vs velocities of the Cascello MASW; (f) Vs velocities of the Amatrice 2D array. Seismic velocity values shown in color scales are expressed in m/s. A detailed list of used geophysical data is shown in table 1.

	NAME	CODE	Vs	Vp	LITHOFACIES	DEPTH (m)
DOWN-HOLE (DH)	Amatrice_DH1	DH1	×	×	✓	50
	Amatrice DH2-San Cipriano	DH2	✓	✓	✓	51
	Amatrice_DH3	DH3	✓	✓	✓	52
	Amatrice_DH4-San Francesco	DH4	✓	✓	✓	37
	Cascello_DH1	DH5	✓	✓	✓	50
	Cornillo_Vecchio_DH1	DH6	✓	✓	✓	20
	Cossito_DH1	DH7	✓	✓	✓	30
	Moletano_DH1	DH8	✓	✓	✓	31
	Retrosi_DH1	DH9	✓	✓	✓	50
	Rocchetta_DH1	DH10	✓	✓	✓	50
	Saletta_DH1	DH11	✓	✓	✓	30
	San_Capone_DH1	DH12	✓	✓	✓	30
	San_Lorenzo_Flaviano_Rio_DH1	DH13	✓	✓	✓	30
	Sant_Angelo_DH1	DH14	✓	✓	✓	40
	Sommati_DH1	DH15	✓	✓	✓	40
MASW	Cascello	MA1	✓	✓	×	100
	Collecreta	MA2	✓	✓	×	30
	Cornillo_Vecchio	MA3	✓	×	×	30
	Prato	MA4	✓	✓	×	90
	Retrosi1	MA5	✓	×	×	30
	Retrosi2	MA6	✓	×	×	40
	Rocchetta	MA7	✓	×	×	35
	S.Lorenzo_Pinaco	MA8	✓	×	×	30
2D ARRAY	AMA03	AR1	✓	×	×	30
	Amatrice	AR2	✓	×	×	150
	CAS08	AR3	✓	×	×	120
	S.Angelo	AR4	✓	✓	×	199
	SAL04	AR5	✓	×	×	37
	SCP01	AR6	✓	×	×	80
	SLO01	AR7	✓	×	×	197
	SLO02	AR8	✓	×	×	35
	Sommati	AR9	✓	✓	×	195
	Milana et al., 2019	AR10	✓	×	×	150
	Sommati transect (point S05)	AR11	✓	×	×	312
	Sommati transect (point S06)	AR12	✓	×	×	259
	Sommati transect (point S07)	AR13	✓	×	×	265
	Sommati transect (point S08)	AR14	✓	×	×	248
	Sommati transect (point S09)	AR15	✓	×	×	208

Table 1: List of used subsoil geological and geophysical data. The extended names and codes of measurement points are reported respectively in the “name” and “code” columns, while the availability of geological and geophysical data is indicated in “Vs”, “Vp”, and “lithofacies” columns (green checks, available data; red crosses, not available data). In the “depth” column the maximum investigation depths are expressed in meters from the ground surface. Locations of the measurement points in figure 5a.

3.2 Data preparation and 3D modeling

Geological and geophysical data have been firstly homogenized in terms geological coding (i.e., stratigraphy and lithofacies), quality checked and geo-referenced to a common Spatial Reference by using a GIS software (Fig. 4a), and finally uploaded into a 3D geological and geophysical modeling software (Fig. 4b).

Firstly, all stratigraphic boundaries (lithofacies surfaces) have been digitized on the geological map and cross-sections (Fig. 6a). Then, the XYZ point file obtained for the digitized horizons, integrated with the lithostratigraphic tops intercepted in core-wells, have been gridded. Lithofacies surfaces have been so created (Fig. 6b), manually edited where required, and finally converted back into XYZ point files. In this way, we obtained denser XYZ point files (Fig. 6c) to better constrain the construction of horizons during the 3D modeling phase (see Figure 3).

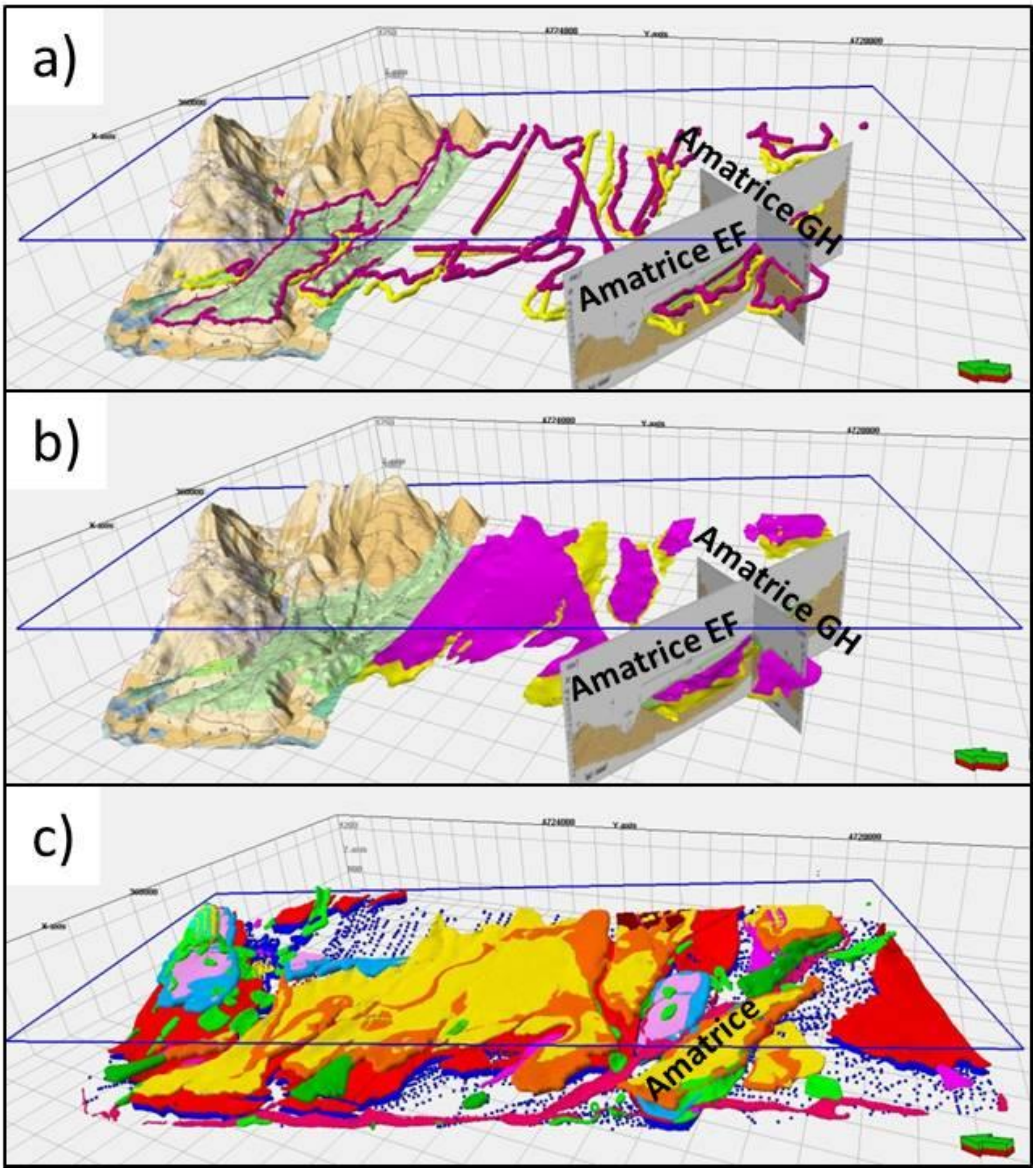

Figure 6: Horizon elaboration workflow. 3D view of digitized horizons: (a) bases of Quaternary sandstones (UASs) (purple points) and conglomerates (UASc) (yellow points) digitized on geological map and cross-sections; (b) gridded surfaces of the UASs and UASc bases; (c) all digitized horizon (XYZ points). Figures a and b show the northern portion of the geological map; two representative geological cross-sections (named Amatrice AB and Amatrice GH) are also reported for illustrating the spatial correlation of the data. See figure 3 to contextualize figures in the workflow.

Faults have been digitized on the geological map and cross-sections (Fig. 7a). The resulting XYZ point files have been finally used as input data to create the fault network (Figs. 3 and 7). It defines faults in the geological model that represents the basis for the development of 3D meshes. The generated faults, in fact, define breaks in the grid, along which the digitized stratigraphic horizons should be offset.

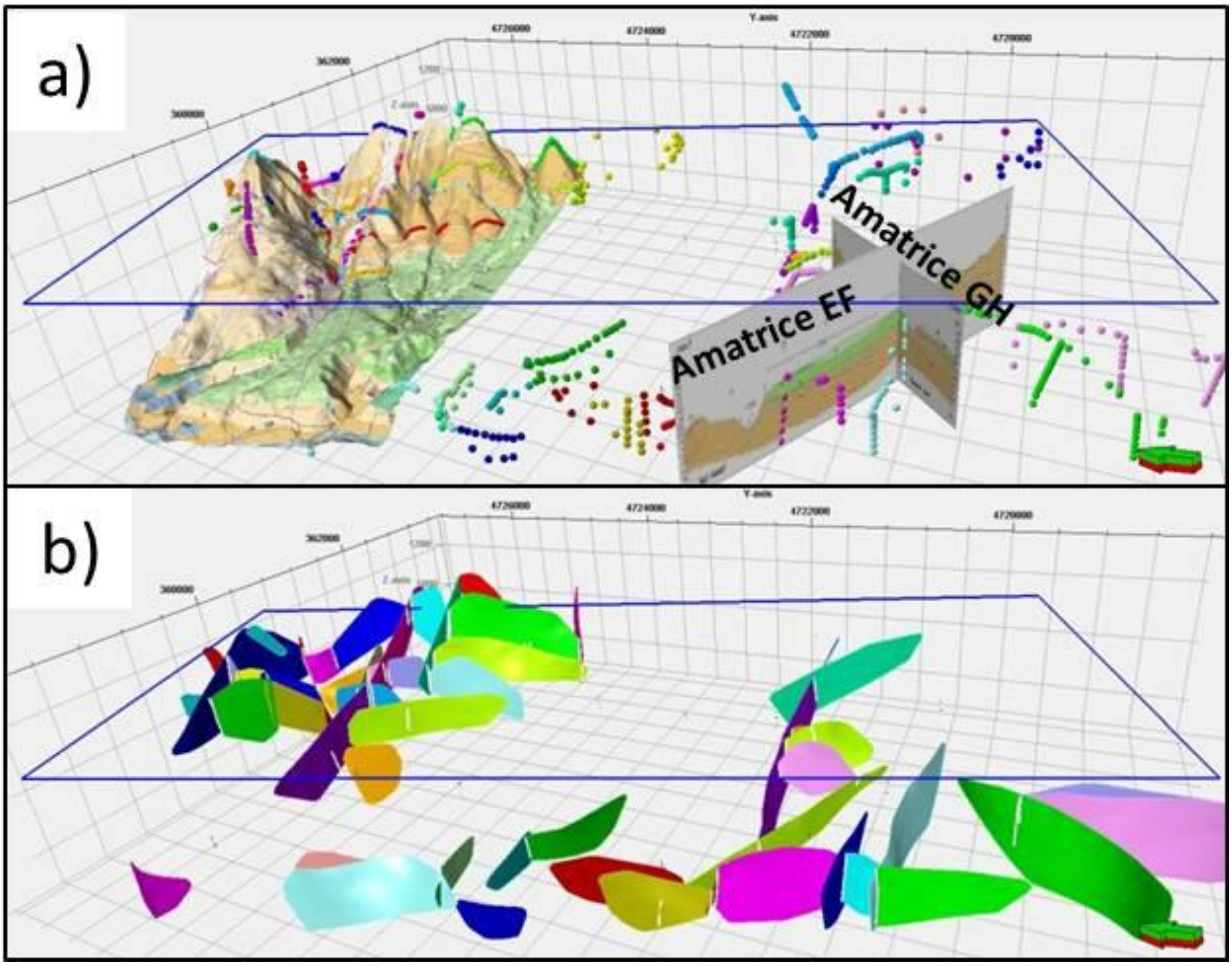

Figure 7: Fault elaboration workflow. (a) 3D view of faults digitized on geological map and cross-sections (XYZ points); (b) 3D view of the processed fault network (solid colored surfaces). In figure the northern portion of the geological map and two representative geological cross-sections (named Amatrice AB and Amatrice GH) are also reported for illustrating the spatial correlation of the data. See figure 3 to contextualize figures in the workflow.

The resulting stratigraphic horizons and faults have been finally checked and, if necessary, corrected to obtain the best fit between their geometry and their outcroppings. Eventually, they have been hierarchized according to the stratigraphic position (for horizons) and cross-cutting relationships (for faults).

The final 3D geological model has been generated with the following procedure. First, the created fault network has been incorporated into a 3D mesh (Fig. 8a), whose average areal resolution has been set to 5 meters. Then, the horizons (Fig. 8b) and the included stratigraphic intervals (Fig. 8c), have been reconstructed. Finally, the resulting stratigraphic intervals have been divided into layers (Fig. 8d).

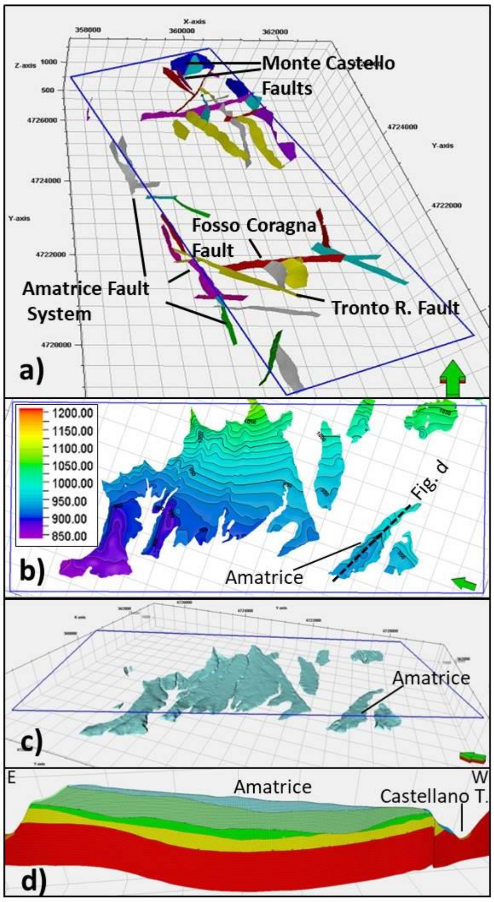

Figure 8: 3D modeling workflow. (a) Fault network generation; (b) Horizon creation (in the figure is shown the contour line map of the base of Quaternary sands); (c) stratigraphic interval creation (in the figure is shown the created Quaternary sandstone zone); (d) layering. See figure 3 to contextualize figures in the workflow.

The 3D geological model has been finally parameterized with the V_s and V_p velocities derived by the DH, MASW (with the associated seismic refraction profiles where available), and 2D array measurements (Fig. 5; Tab. 1). First, we have parameterized the 3D model cells located along the DH, MASW (or seismic refraction profiles for V_p data), and 2D array paths by running a “well log upscaling” process, then, starting from the upscaled cells, the entire 3D model has been populated with the V_s and V_p data following the geological model layering (Fig. 9). In this way, two preliminary geology-based 3D velocity models have been constructed (Figs. 16 and 17). The parameterization of the 3D geological model has been carried out by using a “moving average” interpolation algorithm by Petrel software. The “moving average” algorithm calculates averaged values for cells starting from the input data, to which a weight is associated as a function of the distance from the measurement points. The algorithm is fast and does not generate smaller or bigger values than the minimum and maximum velocity values of the upscaled cells. Furthermore, the "moving average" algorithm, considers the effects of structural (e.g., fault network) and sedimentary (e.g., lithology and anisotropy) conditions on the spatial distribution of geophysical attributes (Shao et al., 2012; Grunis & Khasanov, 2017).

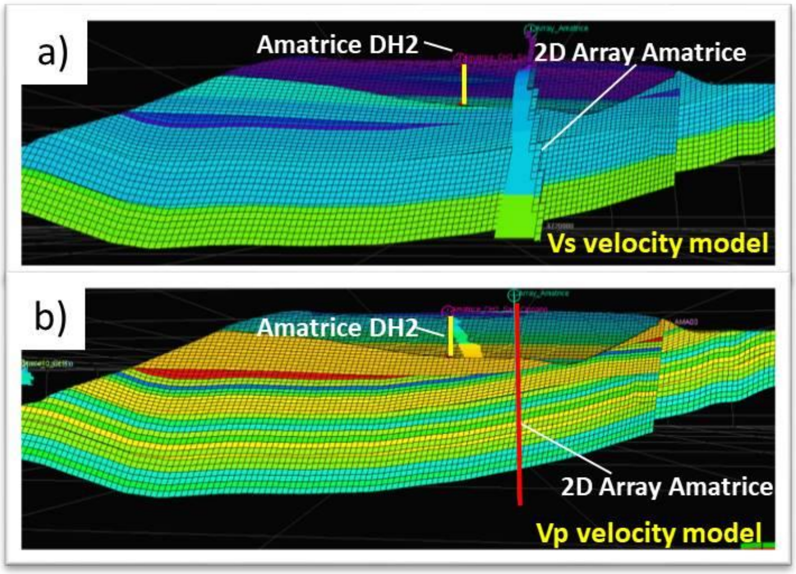

Figure 9: Model parameterization with Vs (a) and Vp (b) values. (a) A section of the Vs velocity model throw the Amatrice plateau with the Amatrice DH2 down-hole (on the section) and the Amatrice 2D array (projected) Vs data; (b) a section of the Vp velocity model throw the Amatrice plateau with the Amatrice DH2 down-hole (on the section) Vp data. On the two models the 3D geological model layers and cells can be observed. See figure 3 to contextualize figures in the workflow.

A preliminary calibration of the realized 3D model has been done by processing the ellipticity curves (see Fäh et al., 2001) of the Rayleigh fundamental mode at two selected sites (hereafter control points).

The procedure of calibration consists of three steps:

1. around each control point, cylindrical 3D meshes (with a radius of 75 m) are extracted (Fig. 10);
2. meshes are organized in seismo-stratigraphy profiles in order to define, for each layer, the thickness in meters, the unit weight in Kg/m^3, the V_p and V_s velocity models in m/s;

3. ellipticity curves of the Rayleigh fundamental mode are computed through the open-source software Geopsy (http://www.geopsy.org/) and compared with the available HVSR curves (Fig. 11).

The selected control points are in the northeastern part of the Amatrice town (i.e., Amatrice historical center, in correspondence of the Milana et al., 2019 2D array), seriously damaged during the 2016-2017 seismic sequence, and in correspondence of the Sommati DH1 site (Fig. 10). This selection was made to focus the attention on some points where the evidence of 2D\3D effects has been demonstrated (Gaudiosi et al., 2021).

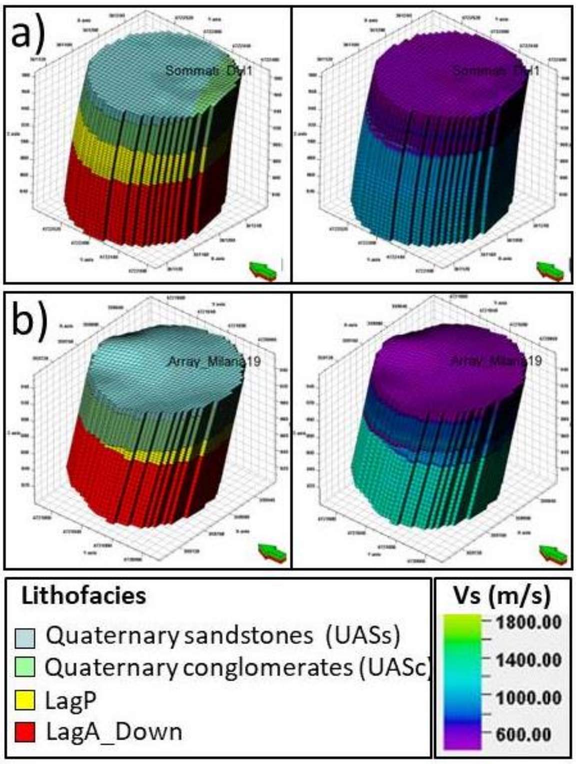

Figure 10: Extracted 3D geological (left) and V_S velocity (right) meshes. The cylindrical meshes (75 m radius) are centered on the Sommati DH1 (a) and Amatrice historical center (in correspondence of the Milana et al., 2019 2D array) (b). Green arrow points north. Site locations are reported in Figure 5a.

The HVSR curves have been automatically scanned to identify the frequencies f at which the maximum amplitudes occur. In this study, the frequency value f_0 is assigned to the lowest fundamental peak of frequency determined for each HVSR curve in the range 1-10 Hz. The f_0 frequency and its standard deviation (according to the SESAME criteria; SESAME, 2004) have been plotted in Fig. 11.

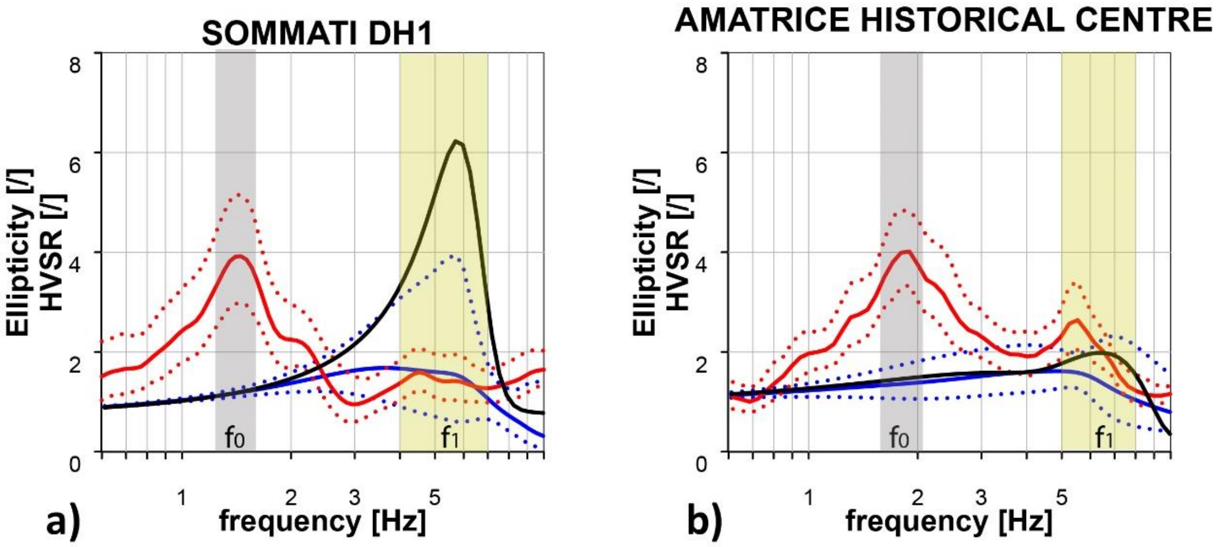

Figure 11: Comparison between ellipticity (blue and black lines) and experimental HVSR curves (red lines) at the chosen control points. The figure shows the comparison of the ellipticity curves at (a) Sommati DH1 and (b) Amatrice historical centre (in correspondence of the Milana et al., 2019 2D array) sites with the experimental HVSR curves recorded at the nearest seismic stations: MZ09 for Sommati DH1 site and CS19 for Amatrice historical centre site. Ellipticity curves are represented considering both the response for the entire cylindrical mesh (blue curves), and a singular vertical profile at its center (black curves). Standard deviations of ellipticity and experimental HVSR curves (dashed blue and red lines, respectively) have been also considered. The grey vertical bands represent the f0 frequency and its standard deviation computed over all the curves from time windows of 50 s length (according to the SESAME criteria; SESAME, 2004). The yellow vertical bands represent the highest amplified frequency band (f_1). The related 3D geological and Vs velocity meshes are shown in figure 10. Locations of the chosen control points and seismic stations are shown in figure 5a.

4 Results

This work provides two georeferenced databases (i.e., a 2D GIS and a 3D databases), a high-resolution 3D geological model, and two preliminary geology-based 3D velocity models (i.e. V_s and V_p velocity models) of the Amatrice Basin.

4.1 Georeferenced databases

Both georeferenced databases (i.e., 2D and 3D) share a common Spatial Reference System (see the appendix section) and classify the data according to their data type (e.g., topography data, geological section, maps, geophysical data, wells, horizons, faults, etc.). The GIS database consists of a 2D georeferenced database that collects morphological (topography contour lines), geological (sections and fault traces, maps, etc.), geophysical (seismic line and MASW traces, HVSR and DH position, etc.), and seismological (epicentral locations of the seismicity of the area) data. The data are subdivided into images (e.g., maps) and vectorial data (i.e., shapefiles). The latter are, in turn, grouped into points, lines, and polygons.

The 3D database contains the previous data that are combined with the related depth information. 3D data can be subdivided into two main groups: primitive data, which consist of the collected data (i.e., well positions, geological cross-sections and maps, velocity data, etc.), and derived data, which consist of the data produced during the various processing phases (i.e., digitized horizons and faults, lithostratigraphic and fault surfaces, etc.) for constructing the 3D geological model.

4.2 The 3D geological model

The performed 3D geological model covers an area of about 24.7 km^2 and extends about 200 meters deep from the topographic surface, with local variations. The area, elongated in NNE-SSW direction, is about 7.8 km long and 3.2 km wide, and extends from Monte Castello to Colle San Lorenzo hamlets, 1.5 km south-east of the Amatrice hamlet (Figs. 4 and 12a). Its western edge roughly follows the orientation of the Tronto River up to the Cornillo Vecchio village and then, southward, follows the Castellano Torrent.

The areal size of cells is 5 meter in the whole area, while the vertical thickness of cells varies from 1 meter for the Quaternary interval, where more data are available and a higher resolution is required, to 3 or 5 meters for the Messinian turbiditic interval (Fig. 8d).

The DEM represents the top surface of the model. From top to bottom, two main stratigraphic successions can be distinguished: the Quaternary continental deposits and the underlying Messinian Laga Formation. The surfaces that delimit the Quaternary continental deposits are erosive, while the underlying ones are conformal (i.e., non-erosive stratigraphic surfaces). The latter represent the interfaces bounding the arenaceous and pelitic intercalations of the Laga Formation.

Quaternary deposits are discontinuously distributed, thus forming isolated patches in the model. On the other hand, the Laga Formation can be traced continuously through the whole studied area. The modeled faults consist of normal faults, which mainly affect the Laga Formation and are generally sutured by the Quaternary deposits, except for rare and limited exposures (Fig. 12).

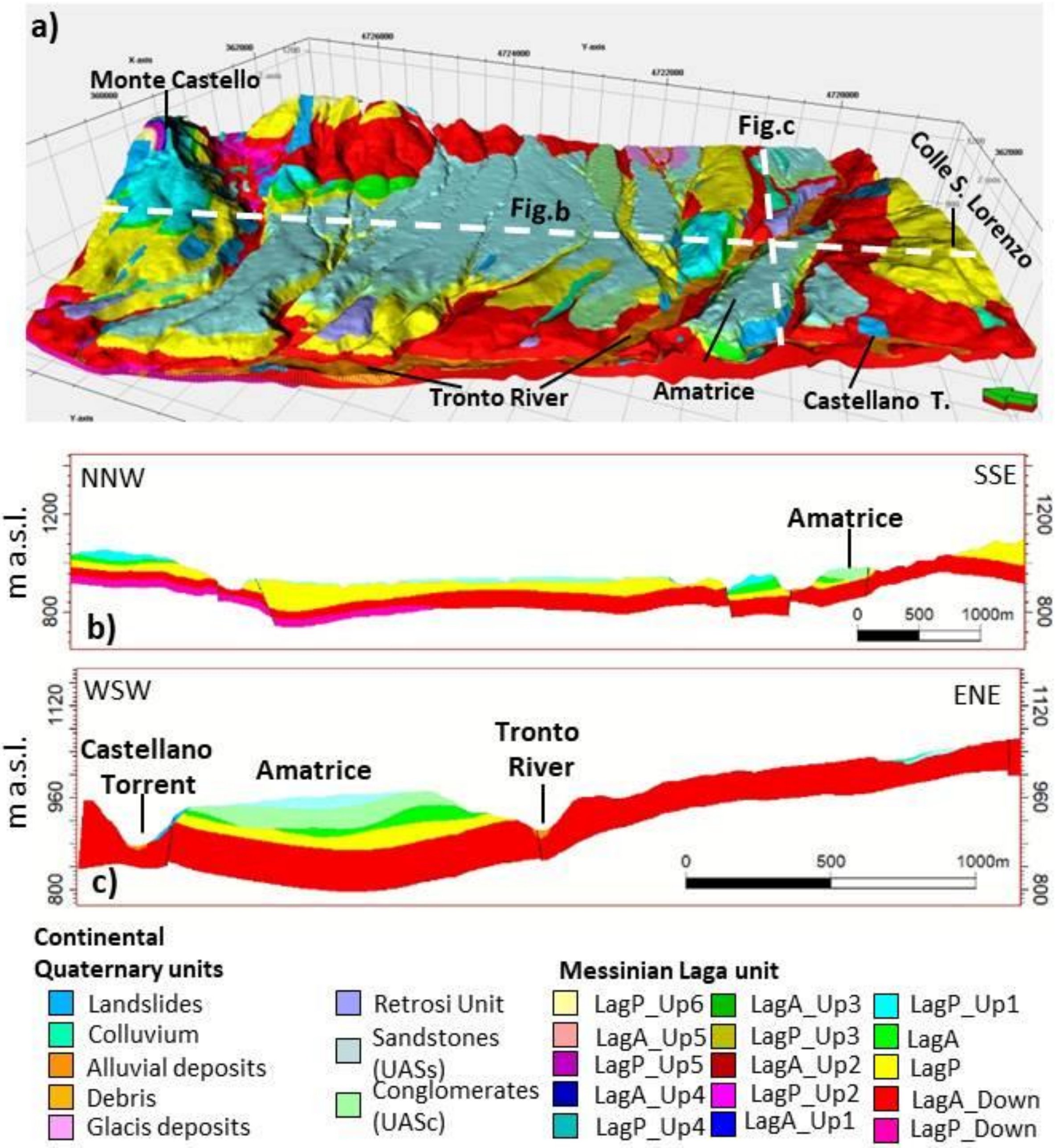

Figure 12: 3D geological model of the study area. (a) View of the 3D geological model; (b) NNW-SSE and (c) WSW-ESE cross-sections through the model (traces in a). Green arrow points north. See figure 3 to contextualize this figure in the workflow.

4.2.1 Quaternary units

The following deposits were modeled for the Quaternary succession: landslide bodies; colluvium; debris; fluvial (e.g., Retrosi Unit) and recent alluvial deposits; Quaternary sandstones and conglomerates (Fig. 13).

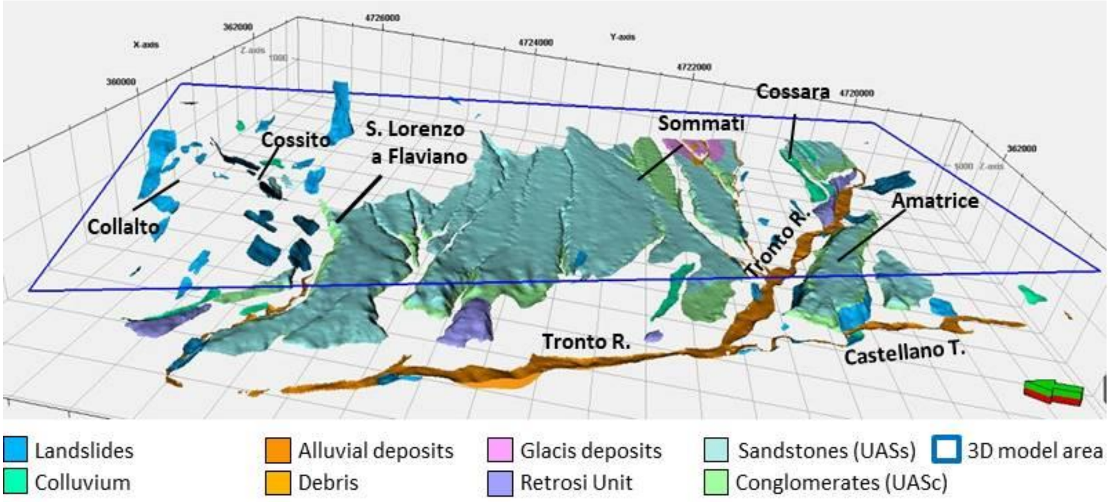

Figure 13: Modeled Quaternary deposits. In this figure a 3D view of the modeled Quaternary deposits is shown. Blue rectangle delimits the modeled area. Green arrow points north.

The landslide bodies, alluvial deposits, sandstones, and conglomerates represent the most widespread Quaternary deposits in the area.

Landslides overlap both the Quaternary and Messinian successions. Their thickness, unraveled by the interpretation of the geological cross-sections, ranges from less than one meter to a few meters. Small to moderate size landslides (~ 0.01 to 0.2 km^2) located at higher altitudes were mapped in the northern portion of the modeled area (surrounding areas of Casale, Collalto, and Cossito hamlets) and in the southern one (surrounding area of Amatrice hamlet). Two medium-sized landslides are located along the north-eastern (~ 0.03 km^2) and south-western (~ 0.06 km^2) slope of the northernmost portion of the Amatrice terrace. The landslide bodies in the middle area, between San Lorenzo a Flaviano and Sommati villages, are instead rare and small (≤ 0.01 km^2).

Alluvial deposits are mainly made up of river deposits that fill the Tronto River and the Castellano Torrent riverbeds. They are located along the western edge of the model and immediately northeast of Amatrice village. Their thickness, defined by the geological sections, is up to a few meters, changing both along and across the riverbed.

Quaternary sands cover a large part of the model area. The most extensive outcrop (~5.6 km^2) is in the central area, where its base descends, as well as the slope, from northeast to southwest, towards the Tronto River (Fig. 8b). Other medium-sized (~ 0.2 to 0.5 km^2) outcrops are present in the Amatrice, Prato-Voceto, and Cossara areas. A limited number of small outcrops (≤ 0.02 km^2) can also be observed in the model. This lithofacies overlaps in part the Quaternary conglomerates and in part the Messinian foredeep deposits. Its average thickness ranges from few meters to about 20-25 meters. In the Amatrice village area, the base of the lithofacies shows an upward concave shape and reaches its maximum thickness (approx. 20 meters) in the middle part of the terrace.

The Quaternary conglomeratic lithofacies interposes between Quaternary sands and Messinian foredeep deposits. It is characterized by a variable thickness ranging from a few meters up to about 30-35 meters. Its base is an erosive surface characterized by culminations and depressions. In the central area, this base shows a general dip from east to west, while in the Amatrice area it shows a general upward concave shape (Fig.14). Quaternary conglomerates and sands are characterized by mostly horizontal internal layering.

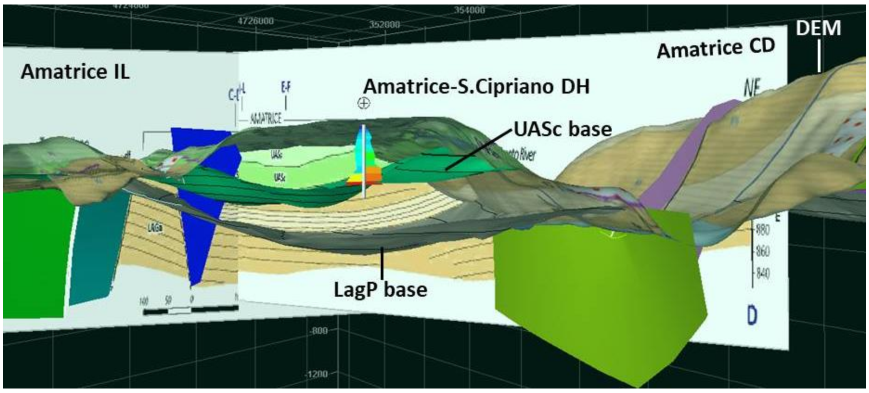

Figure 14: 3D view of the Amatrice subsoil. The figure shows the processed UASc and LagP bases. The upward concave geometry of the stratigraphic horizons is evident. Two geological cross-sections (i.e., Amatrice CD and Amatrice IL), the Amatrice-San Cipriano DH (also named Amatrice DH2) and the associated S-wave (left) and P-wave (right) velocities, the DEM, and some processed faults (solid-colored vertical surfaces) are shown.

4.2.2 Messinian foredeep deposits

The Messinian foredeep deposits of the Laga Formation are made up of an interlayering between arenaceous and pelitic layers. Overall, we reconstructed eight pelitic lithofacies and seven arenaceous ones. Some arenaceous and pelitic intercalations (i.e., LagA and LagP) have been considered as reference horizons to hierarchize and denominate all the Laga intercalations. The name associated to each lithofacies contains both lithological (i.e., "A" for arenaceous and "P" for pelitic) and stratigraphical (i.e., "down" for layers below reference horizons and "up" for layers above reference horizons; numbers, proceeding upwards with respect to the reference horizons, indicate the stratigraphic position of the arenaceous and pelitic intercalations) information (Fig 15).

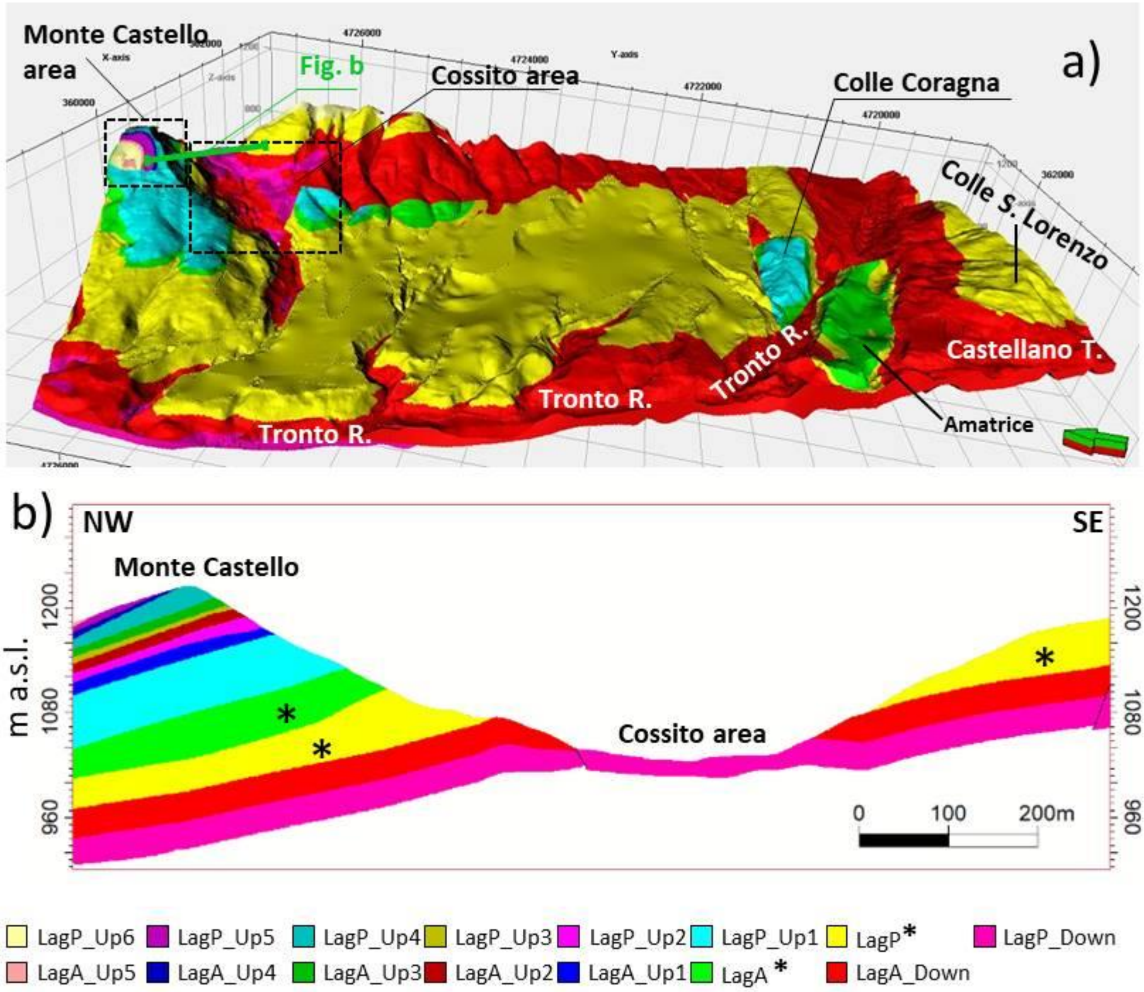

Figure 15: Modeled Laga deposits. (a) 3D view of the modeled Laga deposits. The overlying Quaternary deposits have been switched off. Monte Castello and Cossito areas are shown (black dashed rectangles). Green arrow points north. (b) Geological cross-section across the Monte Castello and Cossito areas (trace in a; green line). In Monte Castello area an upward reduction of the intercalation thickness can be observed. Black asterisks indicate the reference horizons.

The deepest Messinian horizon (i.e., LagA_Down base) and the underlying lithofacies (i.e., LagP_Down layer), identified below the reference horizons, have been modeled exclusively on the basis of the data collected in the Cossito surrounding area, the only area where they crop out (Fig. 15). The LagA layer (reference horizon) widely cropping out in the model area, while the overlying ones sporadically cropping out in some smaller areas (e.g., LagP layer, Amatrice and Monte Castello areas; LagP_Up1 layer, Colle Coragna and Monte Castello areas). The stratigraphically higher Laga portion (i.e., from LagA_Up1 to LagP_Up6 layers), instead, crops out exclusively in Monte Castello area, where layers have been lowered by normal faults bounding the Monte Castello structure. This interval consists of a rapid alternation of thin arenaceous and pelitic intercalations (Fig. 15).

In some cases, the thickness of Messinian lithofacies varies due to the original shape of the sedimentary basin and/or erosional phenomena.

Laga intercalations are overlaid by younger Messinian layers by means of conformal surfaces or by Quaternary continental deposits by means of erosive surfaces.

4.2.3 Faults

The Messinian foredeep deposits appear disarticulated by an extensional fault system located at the hanging wall of a major west-dipping normal fault (i.e., the Gorzano-Laga Fault), to which defines a subsidiary structure (Vignaroli et al., 2020) (Fig. 1). Most of normal faults have been mapped in the southwestern and northeastern portions of the 3D geological model, while the central part (between Rocchetta and Sommati villages) lacks the occurrence of such tectonic structures. However, we cannot exclude the presence of additional faults sealed by the Quaternary continental deposits.

Two main fault trends can be identified: an NNW–SSE and an E-W one (Fig. 8a). When observed, the E-W-striking system systematically cut and dislocates the NNW-SSE-striking one. Fault plains are generally characterized by high dip angles (>60°) and their length varies from a few hundred meters up to a few kilometers.

The NNW-SSE striking normal fault system is observed along the western boundary of the model. This fault system, named Amatrice Fault System, runs along the Tronto River in his northern portion, up to the Cornillo Vecchio village, and along the Castellano Torrent in his southern portion. This fault system is segmented into several portions by some small E-W normal faults (Fig. 8a).

Along some faults a rotational movement of the fault blocks around the intermediate stress axis (σ_2) is observed (scissor faults). The rotation causes the block lifting on one side and its lowering on the other side. In the Monte Castello area, for example, Messinian deposits are lowered northwestwards and raised southeastwards by the activity of the faults bordering the Monte Castello structure, while, in the Colle Coragna area, the Messinian deposits are lowered westwards and raised eastwards by the activity of the Fosso Coragna and the Tronto River faults (Figure 8a). The rotation in both cases gives to the Messinian deposits the aspect of monoclines with different dip with respect to the surrounding deposits.

4.3 3D velocity models

The reconstructed geology-based V_s and V_p velocity models represent a first attempt to parameterize the geological model, aimed at defining the 3D distribution of the geophysical parameters in the modeled geological volume. Starting from the parameterized cells along the DH, MASW (or seismic refraction profiles for V_p data), and 2D array measurement path (upscaled cells), the V_s and V_p velocities populate the entire 3D model with a gradual value variation defined by the adopted “moving average” algorithm following the geological model layering (Figs. 16 and 17).

The V_s model (Fig. 16) is characterized by velocity values that are in a range between 100 m/s (at the top of the SLO01 2D array) and 1667 m/s (at the base of the Amatrice 2D array). They show a general downward increasing, with marked local velocity inversions within the modeled succession. The lowest V_s values (about 100 m/s) are observed in correspondence of the Quaternary continental deposits. In some cases, a sudden increase in V_s values (from 607 m/s to 1170 m/s at 37.7 m depth of the Amatrice DH2-San Cipriano Down-Hole, 2.3 meters above the Quaternary base) occurs near the transition between Quaternary deposits and Messinian foredeep deposits (Figs. 9a, 16b and 16c). The V_s values of the Messinian foredeep deposits vary from a few hundred meters per second up to a maximum of 1667 m/s near the model base, as also recorded at the bottom of the Amatrice 2D array. Within the Messinian succession there are some local velocity inversions, which are likely due to the lithological interlayering of the arenaceous-pelitic succession. Low velocity values are sometimes observed within the uppermost (few meters) layers of the Laga lithofacies (e.g., at the top of the San Capone DH1, V_s = 162 m/s) and interpreted as the effect of weathering.

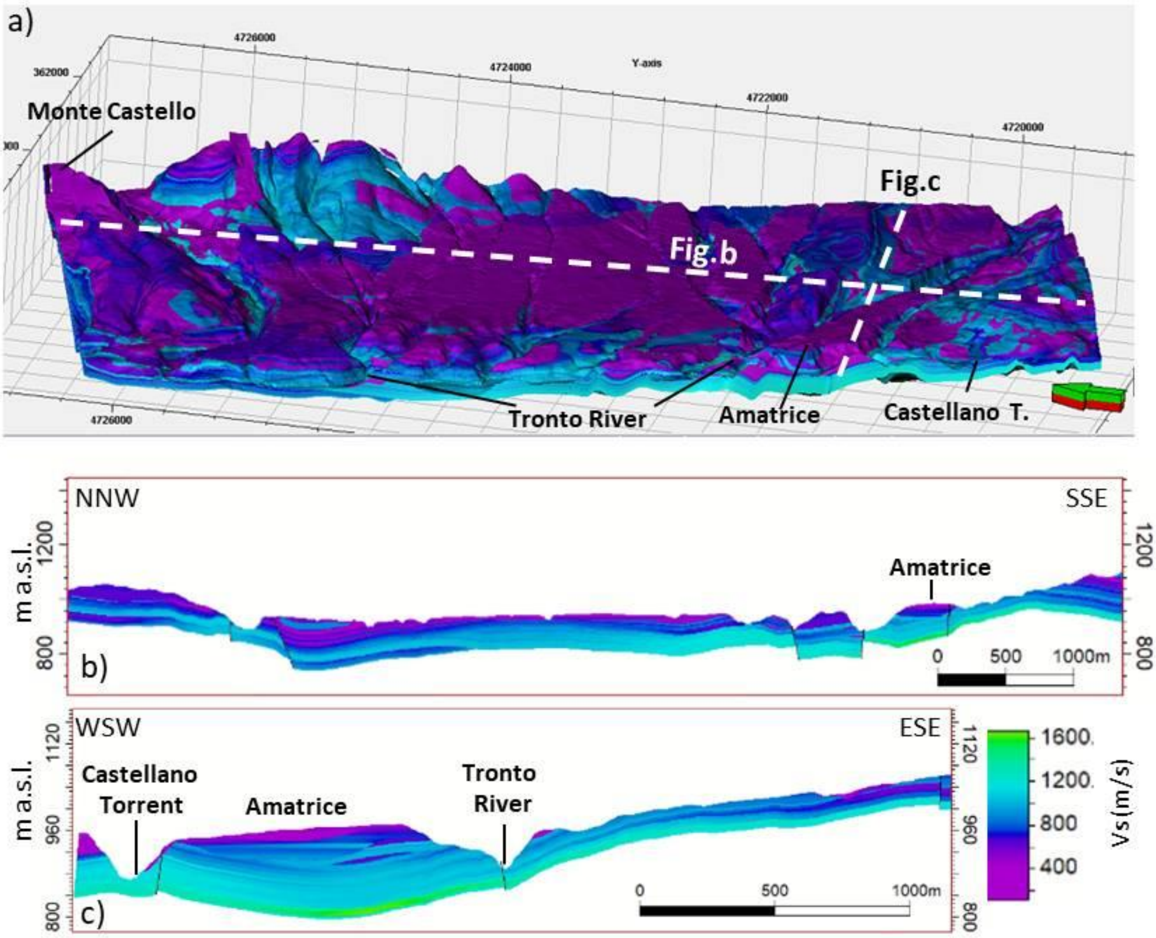

Figure 16: 3D Vs velocity model. (a) View of the 3D Vs velocity model; (b) NNW-SSE and (c) WSW-ENE cross-sections through the Vs velocity model (traces in a). Green arrow points north. See figure 3 to contextualize this figure in the workflow.

The V_P velocity model (Fig. 17) is mainly based on the DH recordings, plus some additional MASW (or seismic refraction profiles) and 2D array data (see table 1). For this reason, the lower part of the V_P model is less constrained compared to the V_s model. V_P values range between 225 m/s (at the top of the S. Angelo 2D array) and 2960 m/s (maximum V_P value recorded the Cossito DH1). In the continental Quaternary units, we can observe a generally downward increasing of V_P values that, in this interval, vary from about 225 m/s to 1800 m/s (e.g., near the Quaternary base in the Amatrice DH2-San Cipriano and Amatrice DH3 Down-Holes). The Messinian foredeep deposits, instead, are characterized by greater V_P values, that approximately range from 317 m/s to 2960 m/s, with several internal velocity inversions. In some areas, where the Laga unit crops out, we can observe low V_P values, like for example at the top of the San Capone DH1 Down-Hole (V_P =317 m/s).

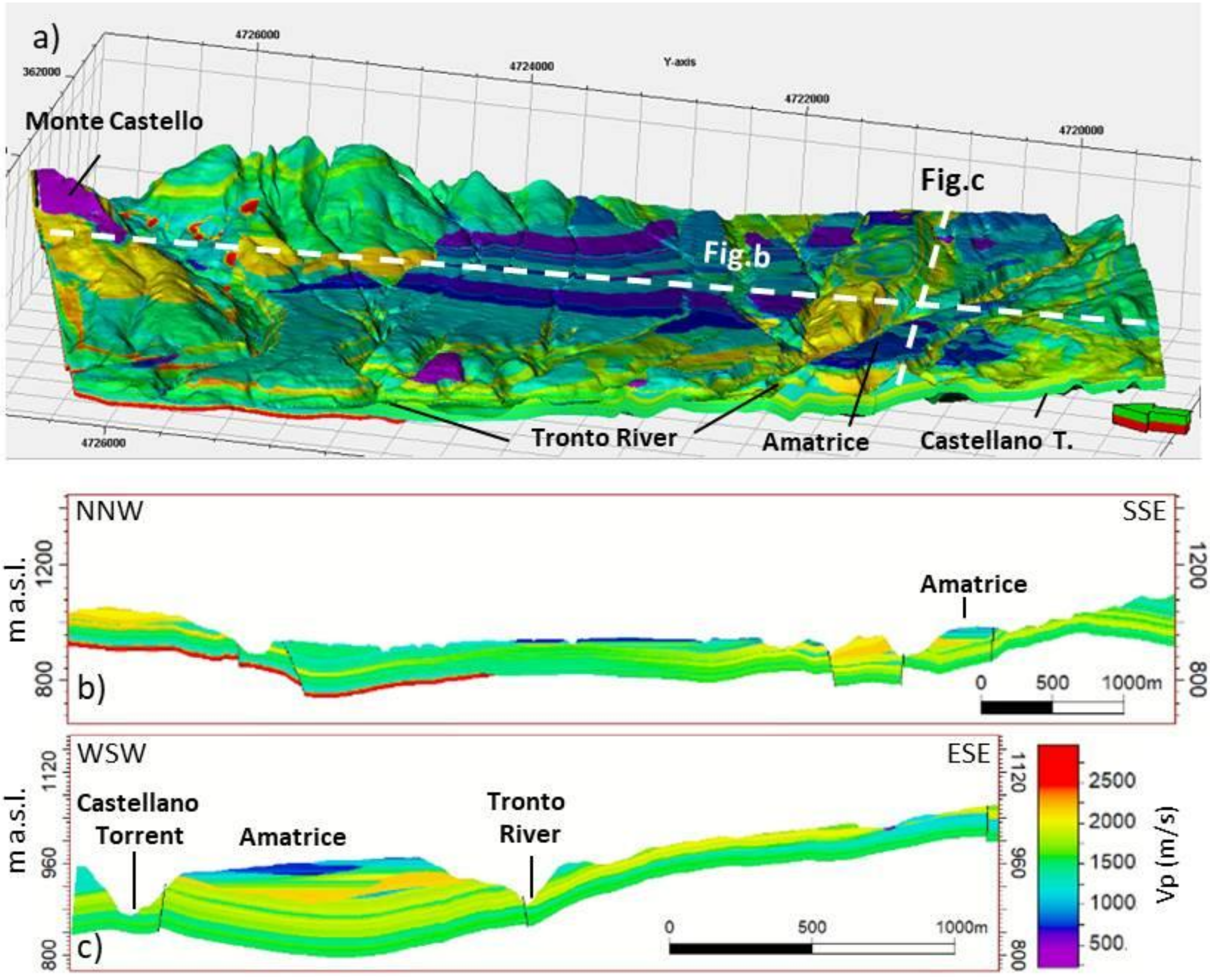

Figure 17: 3D Vp velocity model. (a) View of the 3D Vp velocity model; (b) NNW-SSE and (c) WSW-ENE cross-sections through the Vp velocity model (traces in figure a). Green arrow points north. See figure 3 to contextualize this figure in the workflow.

4.4 Geophysical constrains

The model reliability has been estimated by comparing the experimental HVSR curves, available at the nearest seismic stations (i.e., MZ09 and CS19, localization in Fig. 5a), and the ellipticity curves calculated at the selected control points (i.e., Sommati DH1 and Amatrice historical centre, sites, Fig. 11).

The experimental HVSR curves, recorded at the nearest seismic stations, show two amplified frequency bands: a lowest frequency band (f_0), located between 1 and 2 Hz, with an associated HVSR peak with a value of about 4.2 at the two different control points (grey vertical bands in Fig.11), and a highest frequency band (f_1, yellow vertical bands in Fig.11) ranging between 4.0 and 7.0 Hz, that in the case of Amatrice historical centre is characterized by a broadband behaviour and amplitude values of the HVSR smaller than 2.

The lowest amplified frequency band (f_0) has never been reproduced by the model and the ellipticity curves obtained at Sommati DH1 are characterized by large standard deviations. On the contrary, all the amplification peaks at frequency between 4 and 7 Hz are recognizable in the ellipticity curves. The averaged responses of the modeled ellipticity curves are only slightly underestimated at high frequency (i.e., f_1), attesting the goodness of the model parameterization of the surficial layers above 200 m. In fact, a bias affecting ellipticity amplitudes is expected and does not invalidate the results: the natural noise field contains Love, Rayleigh and body waves, while the calculated ellipticity is generated assuming that the noise field is composed only by Rayleigh waves.

Looking at investigating the influence of lateral variability on the seismic response, ellipticity curves obtained at the center of the two cylindrical meshes were also represented in Fig. 11.

In the two cases, at the centre of each model the ellipticity exceeds the average values ± st. dev.

The case of Sommati site, where the ellipticity is significantly variable inside the modelled volume, leads us to conclude that the geological variability is significant, although the HVSR measurement is few meters away from the exact location of the Down-Hole.

In the historical centre, the variability is less evident, but ellipticity curve at the centre of the model shows a slightly shift of the f_1 frequency respect to the average. The behaviour in this case confirms that pinch-out zones, existing in the areas around the control points, influence the HVSR and the ellipticity modelling, thus affecting also the actual seismic response at the sites.

5 Discussions and conclusions

The 2016-2017 seismic sequence, which violently struck central Italy, put in evidence that more effort should be addressed to the assessment of the seismic hazard in the inner complex basins such as the Amatrice Basin.

Structural and stratigraphic characterization of surface deposits allowed defining the local seismic response (Chiaretti & Nibbi, 2018; EmerTer Project Working Group, 2018; Vignaroli et al., 2019; Hailemikael et al., 2020; Mancini et al., 2020). Despite these studies have been the key for the seismic hazard assessment of the area, they mainly investigate the characteristics of the shallow subsoil layers, hampering a full three-dimensional parametrization of the geological volume affected by the seismic waves. It should be noted that a three-dimensional geological model better approximates geometries and latero-vertical heterogeneities (e.g., thickness, facies changing, structural discontinuities) that induce modifications of the propagating seismic waves, in terms of reflections, refractions, energy absorption, amplifications. For this reason, seismic hazard studies of an area require realistic geological and seismic-velocity models. These models can provide more accurate ground shaking predictions, as confirmed by the seismic hazard assessment studies carried out by Magistrale et al. (1996) and Süss et al. (2001) in the Los Angeles sedimentary basin. The authors proved that geology-based seismic-velocity models allow determining correctly the timing and the amplitude of the arriving waves in earthquake ground-motion simulations.

After the 2016-2017 seismic sequence, a heterogeneous distribution of the damage was observed in the Amatrice hamlet. The historical center, located at the northwest side of a terraced area, was destroyed, while the central and southeastern portion of the village was affected by a lower damage. Milana et al. (2019) highlighted a significant variability in the amplification function in terms of both spectral ratio amplitude and frequency response. In particular, the authors observed a vanishing of the amplification factors at the base of the Amatrice terrace and in central portion of the village, while a strong amplification was observed in both the northwestern and the southeastern edges. These variability in terms of effects highlights the possible contribution of the geological heterogeneity, associated with topographic consequences near the terrace border.

In terms of novelty, our work provedes an accurate geology-based velocity model, which simultaneously considers geological and geophysical characteristics of the modeled volume. The ellipticity curves, elaborated by extracting two cylindrical (75 m radius) V_s velocity meshes from the whole V_s velocity model (Fig. 10), allows us identifying a high amplified frequency band (f_1), between 4.0 and 7.0 Hz, where the calibration is satisfactory. In fact, this frequency band is also amplified in the experimental HVSR curves recorded at the nearest seismic stations (Fig. 11). This demonstrates not only the reliability of the realized geology-based V_s velocity model at the calibrated sites, but also that the amplification of this frequency band origins within the last hundreds of meters, within the modeled volume.

By employing our model in earthquake ground-motion simulations it could also be possible predicting possible focusing and/or amplification effects, due to mechanical and geological features, such as the upward concave geometries reconstructed beneath the Amatrice village (Fig. 14). In this perspective, future research will be carried out.

In the experimental HVSR curves a lower amplified frequency band, f_0, is recognized, but it was never reproduced by means of our model (Fig. 11). The absence of the f_0 peak in the ellipticity curves processed at the chosen sites could be due to: 1) the occurring of 2D/3D effect at low frequency, such as recognized by Gaudiosi et al. (2021) along the Amatrice terrace; 2) the presence of a deeper geological interface and/or mechanical impedance contrast, located below the modeled volume.

Considering the results of our study, we can conclude as follows:

- our geology-based model could help in predicting correctly the amplitude and frequency of arriving seismic waves by calibrating the model in additional scattered points of the Amatrice Basin;
- the proposed model could also help in predicting possible focusing and/or amplification effects by performing earthquake ground-motion simulations;
- a deepening of the model by using and interpreting data reaching greater depths, such as seismic reflection profiles, is necessary to investigate the origin of the lowest amplification frequency band (f_0);
- the proposed method represents a promising missing step between seismic zoning at large scales and microzonation studies, by integrating all the available geological and geophysical information;
- in complex geological contexts, such as the intermountain basins, the availability of geophysical information linking surface and deep data is essential to correctly evaluate the local seismic hazard;
- the proposed approach helps in defining more realistic seismic hazard scenarios and is exploitable in other comparable sectors of the central Apennine.

Appendix

In this work a WGS84-UTM33N Spatial reference (EPSG 32633) has been adopted. For data georeferencing we have used the QGis software (Version 2.18), while, for the realization of the 3D geological model and its parameterization we have used the Petrel software (Version 2016.2), mark of Schlumberger. Ellipticity curves have been modeled by using “gpell” code by geopsy software (http://www.geopsy.org/index.html).

Acknowledgments

This work has been supported by the Institute of Environmental Geology and Geoengineering (IGAG-CNR) of Rome, Italy [Research fellow, conferment document number 01543 dated 3 June 2019] and carried out within the framework of the AMATRIX project (a self-financed project as an application of the RETRACE-3D project). Special thanks to the EmerTer Project Working Group for making available geological and geophysical data underlying this work and for the useful discussions and suggestions.

References

Aldega L., Botti F. & Corrado S. (2007) - *Clay mineral assemblages and vitrinite reflectance in the Laga Basin (central Apennines Italy): what do they record?* Clay and Clay Minerals, 55, 504-518.

Argnani A. & Ricci Lucchi F. (2001) - *Tertiary siliciclastic turbidite systems of the Northern Apennines.* In: G.B. Vai, & I.P. Martini, (Eds.), Anatomy of an Orogen: the Apennines and Adjacent Mediterranean Basins. Kluwer Academic Publishers, 327-350.

Artoni A. (2003) - *Messinian events within the tectono-stratigraphic evolution of the Southern Laga Basin (central Apennines, Italy).* Boll. Soc. Geol. It., 122, 447-465.

Artoni A. (2007) - *Growth rates and two-mode accretion in the outer orogenic wedge-foreland basin system of central Apennine (Italy).* Boll. Soc. Geol. It., 126, 531-556.

Bigi S., Casero P., Corrado S., Milli S., Moscatelli M. & Stanzione O. (2006) - *Geometric framework and thermal history of the Laga basin: constraints for integrated basin analysis.* Abstract, Poster session Ts7.2 XY0592, EGU General Assembly 2006.

Bigi S., Milli S., Corrado S., Casero P., Aldega L., Botti F., Moscatelli M., Stanzione O., Falcini F., Marini M. & Cannata D. (2009) - *Stratigraphy, structural setting and thermal history of the Messinian Laga Basin in the context of Apennine foreland basin system.* J. Med. Earth Sciences, 1, 61-84.

Bigi S., Casero P. & Ciotoli G. (2011) - *Seismic interpretation of the Laga basin; constraints on the structural setting and kinematics of the central Apennines*. Journal of the Geological Society, London, 168, 179–190. doi:10.1144/0016-76492010-084

Billi A. & Tiberti M. (2009) - *Possible causes of arc development in the Apennines, central Italy*. Geological Society of America Bulletin, 121, 1409–1420.

Boccaletti M., Ciaranfi N., Cosentino D., Deiana G., Gelati R., Lentini F., Massari F., Moratti G., Pescatore T., Ricci Lucchi F. & Tortorici L. (1990) - *Palinspastic restoration and paleogeographic reconstruction of the peri-Tyrrhenian area during the Neogene*. Paleogeography Paleoclimatology Paleoecology, 77, 41-50.

Boncio, P., Lavecchia, G. & Pace, B. (2004) - *Defining a model of 3D seismogenic sources for Seismic Hazard Assessment applications: The case of central Apennines (Italy).* Journal of Seismology 8, 407–425. https://doi.org/10.1023/B:JOSE.0000038449.78801.05

Cacciuni A., Centamore E., Di Stefano R. & Dramis F. (1995) - *Evoluzione morfotettonica della conca di Amatrice.* Studi Geologici Camerti, Volume speciale 1995 (2), 95–100.

Casero P. & Bigi S. (2006) - *Deep structure of the Laga Basin.* Abstract, Poster session TS7.2 - XY0591, EGU General Assembly 2006.

[Data set] Castello B., Selvaggi G., Chiarabba C. & Amato A. (2006) - *CSI Catalogo Della Sismicita` Italiana 1981-2002, Version 1.1*. INGV-CNT, Roma.

Cavinato G. P. & De Celles, P. G. (1999) - *Extensional basins in the tectonically bimodal central Apennines fold-thrust belt, Italy: Response to corner flow above a subducting slab in retrograde motion.* Geology, 27, 955–958, doi:10.1130/0091-7613(1999)027<0955:EBITTB>2.3.CO;2

Cavinato, G. P., Carusi, C., Dall'Asta, M., Miccadei, E. & Piacentini, T. (2002) - *Sedimentary and tectonic evolution of Plio-Pleistocene alluvial and lacustrine deposits of Fucino Basin (central Italy).* Sedimentary Geology, 148, 29–59. doi:10.1016/S0037-0738(01)00209-3

Centamore E., Cantalamessa G., Micarelli A., Potetti M., Berti D., Bigi S., Morelli C. & Ridolfi M. (1991) - *Stratigrafia e analisi di facies dei depositi del Miocene e del Pliocene inferiore dell'avanfossa marchigiano-abruzzese e delle zone limitrofe*. Studi Geologici Camerti, vol. spec. 1991/2, 125-131.

Centamore E., Cantalamessa G., Micarelli A., Potetti M., Berti D., Bigi S., Morelli C. & Ridolfi M. (1992) - *Carta geologica del bacino della Laga e del Cellino e delle zone limitrofe.* S.EL.CA., Firenze.

Chiaraluce L., Valoroso L., Piccinini D., Di Stefano R. & De Gori P. (2011) - *The anatomy of the 2009 L'Aquila normal fault system (central Italy) imaged by high resolution foreshock and aftershock locations.* J. Geophys. Res., 116 (B12), doi: 10.1029/2011JB008352.

Chiaraluce, L., Di Stefano, R., Tinti, E., Scognamiglio, L., Michele, M., Casarotti, E., Cattaneo M., De Gori P., Chiarabba C., Monachesi G., Lombardi A., Valoroso L., Latorre D. & Marzorati, S. (2017). *The 2016 central Italy seismic sequence: A first look at the mainshocks, aftershocks, and source models*. Seismological Research Letters, 88(3), 757–771. https://doi.org/10.1785/0220160221

Chiaretti F. & Nibbi L. (2018) - *Microzonazione Sismica di Livello 3 del Comune di Amatrice ai sensi dell'ordinanza del Commissario Straordinario n°24 registrata il 15 maggio 2017 al n°1065*. Comune di Amatrice, 2018. http://www.regione.lazio.it/prl_ambiente/?vw=contenutidettaglio&id=238 (accessed 15 February 2021)

Cosentino D., Cipollari P., Marsili P. & Scrocca D. (2010) - *Geology of the central Apennines: a regional review.* In: Beltrando M., Peccerillo A., Mattei M., Conticelli S. & Doglioni C. (Eds.), The Geology of Italy: tectonics and life along plate margins, Journal of the Virtual Explorer, volume 36, paper 12, doi: 10.3809/jvirtex.2010.00223.

Del Gaudio V., Wasowski J., Pierri P.,1 Moretti A. & Ferrini G. (2021) - *Multitemporal analysis of ambient noise polarization to characterize site response in the town of Amatrice, shattered by the 2016 central Italy earthquake*. Geophys. J. Int. (2021) 224, 739–759. doi: 10.1093/gji/ggaa335

Deschamps A., Courboulex F., Gaffet S., Lomax A., Virieux J., Amato A., Azzara A., Castello B., Chiarabba C., Cimini G.B., Cocco, M., Di Bona M., Margheriti L., Mele F., Selvaggi G., Chiaraluce L., Piccinini D. & Ripepe M. (2000) - *Spatio-temporal distribution of seismic activity during the Umbria-Marche* crisis 1997. J. Seismol., 4, 377–386.

Di Bucci D., Buttinelli M., D'Ambrogi C., Scrocca D. & RETRACE-3D Working Group (2021) - *RETRACE-3D project: a multidisciplinary collaboration to build a crustal model for the 2016-2018 central Italy seismic sequence*. Bollettino di Geofisica Teorica ed Applicata, 62 (1), 1-18, doi: 0.4430/bgta0343.

Doglioni C. (1991) - *A proposal of kynematic modelling for west-dipping subductions - Possible application to the Tyrrhenian-Apennines system*. Terra Nova, 3, 423-434.

EmerTer Project Working Group (2018) - *Report relativo all'Accordo ai sensi dell'art. 15 Legge 7 agosto 1990 n. 241, e dell'art.6 della Legge 24 febbraio 1992, n. 225 tra il Dipartimento della Protezione Civile e l'Istituto di Geologia Ambientale e Geoingegneria del Consiglio Nazionale delle Ricerche per il supporto alle attività della DICOMAC di Rieti e della Struttura di Missione, 2018*. Prot. CNR IGAG n. 359 del 30/01/2018.

Fäh D., Kind F. & Giardini D. (2001) – *A theoretical investigation of average H/V rations*. Geophysical Journal International, 145, 535-549.

Galadini F., 1999. *Pleistocene changes in the central Apennine fault kinematics: A key to decipher active tectonics in central Italy*. Tectonics, 18,5,, 877-894 https://doi.org/10.1029/1999TC900020.

Galadini, F. & Galli, P. (2003) - *Paleoseismology of silent faults in the central Apennines (Italy): the Mt. Vettore and Laga Mts. faults.* Annals of Geophysics, 46(5), 815-836.

Galli P., Peronace E. & Tertulliani A. (2016) - *Rapporto sugli effetti macrosismici del terremoto del 24 Agosto 2016 di Amatrice in scala MCS*. Rapporto congiunto DPC, CNR-IGAG, INGV, Roma. doi: 10.5281/zenodo.161323

Gaudiosi I., Simionato M., Mancini M., Cavinato G.P., Coltella M., Razzano R., Sirianni P., Vignaroli G., Moscatelli M. (2021) - *Evaluation of site effects at Amatrice (central Italy) after the August 24th, 2016, Mw6.0 earthquake.* Soil Dynamics and Erth. Eng. 144. https://doi.org/10.1016/j.soildyn.2021.106699

Giaccio, B., Galli P., Messina P., Peronace E., Scardia G., Sottili G., Sposato A., Chiarini E., Jicha B. & Silvestri S. (2012) - *Fault and basin depocenter migration over the last 2 Ma in the L'Aquila 2009 earthquake region, central Italian Apennines*. Quaternary Sci. Rev. 56, 69–88. doi:10.1016/j.quascirev.2012.08.016

Grunis E.G. & Khasanov D.I. (2017) - *Reserves calculation using the volume and probability methods with the aid oh Petrel-2013 program package*. Methodology of prospecting and exploration of oil and gas fields, 5, 113-118.

Hailemikael S., Amoroso S. & Gaudiosi I. (2020) - *Guest editorial: seismic microzonation of Central Italy following the 2016–2017 seismic sequence*. Bull Earthquake Eng 18, 5415-5422. https://doi.org/10.1007/s10518-020-00929-6

Herrmann R.B., Malagnini L. & Munafò I. (2011) - *Regional moment tensor of the 2009 L'Aquila earthquake sequence*. Bull. Seismol. Soc. Am. 101 (3), 975–993.

Improta L., Latorre D., Margheriti L. et al. (2019) - *Multi-segment rupture of the 2016 Amatrice-Visso-Norcia seismic sequence ,central Italy, constrained by the first high-quality catalog of Early Aftershocks.* Sci Rep 9, 6921. https://doi.org/10.1038/s41598-019-43393-2

[Data set] ISIDe Working Group (2007) - *Italian Seismological Instrumental and Parametric Database (ISIDe).* Istituto Nazionale di Geofisica e Vulcanologia (INGV).

https://doi.org/10.13127/ISIDE

Koopman, A. (1983) - *Detachment tectonics in the central Apennines*. Geological Ultraiectina, 30, 1–155.

Lavecchia G., Adinolfi G., De Nardis M., Ferrarini F., Cirillo D., Brozzetti F., De Matteis R., Festa G. & Zollo A. (2017) - *Faulting model for the largest aftershock of the L'Aquila 1 2009 sequence and implications for unknown active extensional sources in central Italy*. Terra Nova 29, 77–89, doi: 10.1111/ter.12251.

Lucente F.P., De Gori P., Margheriti L., Piccinini D., Di Bona M., Chiarabba C. & Agostinetti N.P. (2010) - *Temporal variation of seismic velocity and anisotropy before the 2009 Mw 6.3 L'Aquila earthquake, Italy*. Geology 38 (11), 1015–1018.

Malinverno A. & Ryan W.B.F. (1986) - *Extension In the Tyrrhenian sea and shortening in the Apennines as result of arc migration driven by sinking of the lithosphere*. Tectonics, 5, 227-245.

Magistrale H., McLaughlin K. & Day S. (1996) - *A geology-based 3D velocity model of the Los Angeles basin sediments*. Bulletin of the Seismological Society of America, 86 (4), 1161–1166.

Mancini M., Cavuoto G., Pandolfi L., Petronio C., Salari L. & Sardella R. (2012) - *Coupling basin infill history and mammal biochronology in a Pleistocene intramontane basin: The case of western L'Aquila Basin (central Apennines, Italy)*. Quaternary International, 267, 62–77. doi:10.1016/j.quaint.2011.03.020

Mancini M., Vignaroli G., Bucci F., Cardinali M., Cavinato G. P., Giallini S., Moscatelli M., Polpetta F., Putignano M. L., Santangelo M. & Sirianni P. (2020). *New stratigraphic constraints for the Quaternary source-tosink history of the Amatrice Basin (central Apennines, Italy).* Geol. J., 1–26. doi: 10.1002/gj.3672

Manzi V., Lugli S., Ricci Lucchi F. & Roveri M. (2005) - *Deep-water clastic evaporites deposition in the Messinian Adriatic foredeep (Northern Apennines, Italy): did the Mediterranean ever dry out?*. Sedimentology, 52, 875-902.

Marini M., Milli S., Ravnås R. & Moscatelli M. (2015) - *A comparative study of confined vs. semi-confined turbidite lobes from the Lower Messinian Laga Basin (central Apennines, Italy): implications for assessment of reservoir architecture*. Marine and Petroleum Geology, 63, 142-165. doi:10.1016/j.marpetgeo.2015.02.015

Marini M., Felletti F., Milli S., & Patacci M. (2016) - *The thick-bedded tail of turbidite thickness distribution as a proxy for flow confinement: Examples from tertiary basins of central and northern Apennines (Italy).* Sedimentary Geology, 341, 96–118.

https://doi:10.1016/j.sedgeo.2016.05.006

Mazzieri I., Stupazzini M., Guidotti R., Smerzini C. (2013) - *SPEED: Spectral Elements in Elastodynamics with Discontinuous Galerkin: a non-conforming approach for 3D multi-scale problems*. International Journal for Numerical Methods in Engineering 95, 12, 991–1010.

Michele M., Chiaraluce L., Di Stefano R. & Waldhauser F. (2020) - *Fine-scale structure of the 2016-2017 central Italy Seismic Sequence from data recorded at the Italian National Network.* Journal of Geophysical Research - Solid Earth. 10.1029/2019JB018440

Milana G., Cultrera G., Bordoni P., Bucci A., Cara F., Cogliano R., Di Giulio G., Di Naccio D., Famiani D., Fodarella A., Mercuri A., Pischiutta M., Pucillo S., Riccio G. & Vassallo M. (2019). *Local site effects estimation at Amatrice (central Italy) through seismological methods*. Bulletin of Earthquake Engineering, 1-27. https://doi.org/10.1007/s10518-019-00587-3

Milli S., Moscatelli M., Stanzione O. & Falcini F. (2007) - *Sedimentology and physical stratigraphy of the Messinian turbidite deposits of the Laga Basin (central Apennines, Italy).* Boll. Soc. Geol. It., 126, 255-281.

Milli S., Moscatelli M., Marini M. & Stanzione O. (2009) - *The Messinian turbidite deposits of the Laga basin (central Apennines, Italy).* In: Pascucci V., Andreucci S. (Eds.), Field Trip Guide Book, Post-conference trip FT12, 27th IAS Meeting of Sedimentology Alghero, September 20-23, 2009, Sassari (Italy), 279-297.

Moscatelli M. (2003) - *La sedimentazione torbiditica e le sue relazioni con quella fluvio-deltizia nel sistema d'avanfossa alto-miocenico dell'Appennino centro-meridionale*. Ph.D. Thesis, Università di Roma "La Sapienza".

Moscatelli M., Milli S., Stanzione O., Marini M., Gennari G. & Vallone R. (2004) - *I depositi torbiditici del Messiniano inferiore dell'Appennino centrale: bacino del Salto-Tagliacozzo e della Laga (Lazio, Abruzzo, Marche).* II Congresso GeoSed, Roma 2004, Libro guida dell'escursione post-congresso.

Moscatelli, I. Gaudiosi, R. Razzano, G. Lanzo, L. Callisto (2020) *Modellazione numerica tridimensionale della risposta sismica dell'abitato di Amatrice.* Capitolo 2.1: Progetto SISMI-DTC Lazio. Conoscenze e innovazioni per la ricostruzione e il miglioramento sismico dei centri storici del Lazio. https://doi.org/10.2307/j.ctv18phgdk

Mutti E. & Ricci Lucchi F. (1972) - *Le torbiditi dell'Appennino settentrionale: introduzione all'analisi di facies.* Mem. Soc. Geol. It., 11, 161-199.

Mutti E., Nilsen T.H. & Ricci Lucchi F. (1978) - *Outer fan depositional lobes of Laga Formation (Upper Miocene and Lower Pliocene), east central Italy*. In: Stanley D.J. & Kelling G., (Eds.), Sedimentation in submarine canyons, fans and trenches. Downed, Hutchinson & Ross, 210-223.

Mutti E. & Sonnino M. (1981) - *Compensation cycles: a diagnostic features of turbidite sandstone lobes*. In: Valloni R., Colella A., Sonnino M., Mutti E., Zuffa G.G. & Ori G.G. (Eds.) IAS 2nd European Regional Meeting, Bologna, Abstract 120-123.

Nocentini M., Asti R., Cosentino D., Durante F., Gliozzi E., Macerola L. & Tallini M. (2017) - *Plio-Quaternary geology of L'Aquila - Scoppito Basin (central Italy).* Journal of Maps, 13 (2), 563–574. doi:10.1080/17445647.2017.1340910

Patacca E., Sartori R. & Scandone P. (1990) - *Tyrrhenian basin and Apenninic Arcs: Kinematic relations since late Tortonian times*. Mem. Soc. Geol. It., 45, 425-451.

Pizzi A., Di Domenica A., Gallovič F., Luzi L. & Puglia R. (2017) - *Fault segmentation as constraint to the occurrence of the main shocks of the 2016 central Italy seismic sequence*. Tectonics, 36, 2370–2387. https://doi. org/10.1002/2017TC004652

Porreca M., Minelli G., Ercoli M., Brobia A., Mancinelli P., Cruciani F., Giorgetti C., Carboni F., Mirabella F., Cavinato G.P., Cannata A., Pauselli C. & Barchi M. R. (2018). *Seismic reflection profiles and subsurface geology of the area interested by the 2016–2017 earthquake sequence (central Italy).* Tectonics 37, 1116–1137. https://doi: 10.1002/2017TC004915

Pucci S., Villani F., Civico R., Pantosti D., Del Carlo P., Smedile A., De Martini P.M., Pons Branchu E. & Gueli A., (2015) - *Quaternary geology of the Middle Aterno Valley, 2009 L'Aquila earthquake area (Abruzzi Apennines, Italy)*. Journal of Maps, 11(5), 689–697. doi:10.1080/17445647.2014.927128

Razzano R., Gaudiosi I., Moscatelli M., Luigi C., Lanzo G., Martini G., Hailemikael S. (2020) *Modelling the three-dimensional site response in the village of Amatrice, Central Italy.* Proceedings of the EGU Assembly, EGU2020-22483, https://doi.org/10.5194/egusphere-egu2020-22483

RETRACE-3D Working Group (2021) - *RETRACE-3D: centRal italy EarThquakes integRAted Crustal modEl. Rapporto finale di progetto*. Eds. INGV, ISPRA, CNR-IGAG, DPC. Roma, pp. 100. doi: 10.5281/zenodo.4604940

Ricci Lucchi F. (1986) - *The Oligocene to recent foreland basin of the Northern Apennines*. In: Allen P.A. & Homewood P., (Eds.). Foreland basins. IAS Spec. Publ., 8, 105-139.

Ripepe M., Piccinini D. & Chiaraluce L. (2000) - *Foreshock sequence of September 26th, 1997 Umbria-Marche earthquakes*. J. Seismol., 4 (4), 387–399.

Roveri M., Bassetti M.A. & Ricci Lucchi F. (2001) - *The Mediterranean Messinian salinity crisis: an Apennine foredeep perspective.* Sed. Geol., 140, 201-214.

Roveri M., Ricci Lucchi F., Lucente C.C., Manzi V. & Mutti E. (2002) - *Stratigraphy, facies and basin fill hystory of the Marnoso-Arenacea Formation*. In: Mutti E., Ricci Lucchi F. & Roveri M. (Eds.), Revisiting turbidites of the Marnoso-arenacea Formation and their basinmargin equivalents: problems with classic models. 64th EAGE Conference & Exhibition. Excursion Guidebook, University of Parma and ENI, AGIP Division, 1-26.

Roveri M., Manzi V., Ricci Lucchi F. & Rogledi S. (2003) - *Sedimentary and Tectonic evolution of the Vena del Gesso Basin (Northern Apennines, Italy): implications for the onset of the Messinian salinity crisis*. Geol. Soc. Am. Bull., 115, 387-405.

[Data set] Rovida A., Locati M., Camassi R., Lolli B. & Gasperini P. (2019) - *Catalogo Parametrico dei Terremoti Italiani (CPTI15), versione 2.0*. Istituto Nazionale di Geofisica e Vulcanologia (INGV). https://doi.org/10.13127/CPTI/CPTI15.2

[Data set] Rovida A., Locati M., Camassi R., Lolli B. & Gasperini P. (2020) - *The Italian earthquake catalogue CPTI15.* Bulletin of Earthquake Engineering. https://doi.org/10.1007/s10518-020-00818-y

Scisciani V. & Montefalcone R. (2005) - *Evoluzione neogenico-quaternaria del fronte della catena centro-appenninica: vincoli dal bilanciamento sequenziale di una sezione geologica regionale.* Boll. Soc. Geol. It., 124, 579-599.

Scognamiglio L., Tinti E., Michelini A., Dreger D.S., Cirella A., Cocco M., Mazza S. & Piatanesi A. (2010) - *Fast determination of moment tensors and rupture history: What has been learned from the 6 April 2009 L'Aquila earthquake sequence.* Seismol. Res. Lett., 81 (6), doi:10.1785/gssrl.81.6.892.

Scognamiglio,L., Tinti E. & Quintiliani M. (2016) - *The first month of the 2016 Amatrice seismic sequence: Fast determination of time domain moment tensors and finite fault model analysis of the ML 5.4 aftershock.* Ann. Geophys. 59, doi: 10.4401/ag-7246.

SESAME (2004) - *Guidelines for the implementation of the H/V spectral ratio technique on ambient vibrations: measurements, processing and interpretation*. SESAME European research project WP12 - Deliverable D23.12, European Commission - Research General Directorate, Bruxelles, Belgium.

Shao Y., Zheng A., He Y. & Xiao K. (2012) - *3D geological modeling under extremely, complex geological conditions*. J. Comput, 3, 699-705.

Smerzini C., Pitilakis *K.* (2018) - *Seismic risk assessment at urban scale from 3D physics-based numerical modeling: the case of Thessaloniki.* Bull Earthquake Eng 16, 2609–2631https://doi.org/10.1007/s10518-017-0287-3

Stanzione O., Milli S., Moscatelli M. & Falcini F. (2006) - *Tectonic and climate control on turbidite sedimentation: the Messinian deposits of the Laga Formation (Central Italy).* Abstract volume, Joint SEPM/Geological Society of London Conference: External controls on deep water depositional systems, climate, sea-level and sediment flux. London, 27-29 March 2006, 75-76.

Süss M.P., Shaw J. H.; Komatitsch D.; Tromp J. (2001) - *3D Velocity and Density Model of the Los Angeles Basin and Spectral Element Method Earthquake Simulations.* American Geophysical Union, Fall Meeting 2001, abstract id. S11A-0549

Tiberi Romano C. (1639) - *Nuova e vera relazione del terribile e spaventoso terremoto successo nella Città della Matrice e suo Stato*, Roma.

Valoroso, L., Chiaraluce L., Piccinini D., Di Stefano R., Schaff D. & Waldhauser F. (2013) - *Radiography of a normal fault system by 64,000 high-precision earthquake locations: The 2009 L'Aquila (central Italy) case study*. J. Geophys. Res., 118 (3), 1156–1176.

Vignaroli G., Mancini M., Bucci F., Cardinali M., Cavinato G.P., Moscatelli M., Putignano M.L., Sirianni P., Santangelo M., Ardizzone F., Cosentino G., Di Salvo C., Fiorucci F., Gaudiosi I., Giallini S., Messina P., Peronace E., Polpetta F., Reichenbach P., Scionti V., Simionato M.& Stigliano F. (2019) - *Geology of the central part of the Amatrice Basin (central Apennines, Italy)*. Journal of Maps, 15 (2), 193-202. doi: 10.1080/17445647.2019.1570877

Vignaroli G., Mancini M., Brilli M., Bucci F., Cardinali M., Giustini F., Voltaggio M., Yu T.-L. & Shen C.-C. (2020) - *Spatial‐ temporal evolution of extensional faulting and fluid circulation in the Amatrice Basin (central Apennines, Italy) during the Pleistocene*. Frontiers in Earth Science, 8, 130. https://doi.org/10.3389/feart.2020.00130

Wathelet, M (2005) - *Array recordings of ambient vibrations: surface-wave inversion*. PhD Dissertation, Liège University, 177p.